Wapl repression by Pax5 promotes V gene recombination by *Igh* loop extrusion

Louisa Hill[1], Anja Ebert[1], Markus Jaritz[1], Gordana Wutz[1], Kota Nagasaka[1], Hiromi Tagoh[1,2], Daniela Kostanova-Poliakova[1], Karina Schindler[1], Qiong Sun[1], Peter Bönelt[1], Maria Fischer[1], Jan-Michael Peters[1] and Meinrad Busslinger[1,#]

[1] Research Institute of Molecular Pathology (IMP), Vienna Biocenter (VBC), Campus-Vienna-Biocenter 1, A-1030 Vienna, Austria

Present address:
[2] Ludwig Institute for Cancer Research, University of Oxford, Oxford OX 7DQ, UK

Running title: Pax5 suppresses Wapl to promote *Igh* recombination

Key words: Pax5, Polycomb repressive complex 2, suppression of Wapl, loop extrusion, *Igh* recombination

ORCID account (Busslinger): http://orcid.org/0000-0002-9111-9351
ORCID account (Peters): htpp://orcid.org/0000-0003-2820-3195

[#] To whom correspondence should be addressed:
phone: (+43/1) 797 30 – 3150 fax: (+43/1) 797 30 – 223150
e-mail: busslinger@imp.ac.at

Abstract

Nuclear processes like V(D)J recombination are determined by the three-dimensional organization of chromosomes in multiple layers, including the compartments[1] and topologically associated domains (TADs)[2,3] consisting of chromatin loops[4]. TADs are formed by chromatin loop extrusion[5-7], which depends on the ring-shaped cohesin complex[8-10] with its loop extrusion function[11,12]. The cohesin-release factor Wapl[13,14] instead restricts loop extension[10,15]. The generation of a diverse antibody repertoire, providing humoral immunity to pathogens, requires the participation of all V genes in V(D)J recombination[16], which depends on contraction of the 2.8-Mb-long immunoglobulin heavy-chain (*Igh*) locus by Pax5[17,18]. How Pax5 controls *Igh* contraction in pro-B-cells is, however, unknown. Here, we demonstrate that locus contraction is caused by loop extrusion across the entire *Igh* locus. Notably, the expression of Wapl is repressed by Pax5 specifically in pro-B and pre-B-cells, which facilitates extended loop extrusion by increasing the residence time of cohesin on chromatin. Pax5 mediates the transcriptional repression of *Wapl* through a single Pax5-binding site by recruiting the Polycomb repressive complex 2 to induce bivalent chromatin at the *Wapl* promoter. Reduced Wapl expression causes global alterations in the chromosome architecture, indicating that the potential to recombine all V genes entails structural changes of the entire genome in pro-B-cells.

Introduction

The mouse *Igh* locus is composed of a 0.26-Mb-long 3' proximal region consisting of 13 D_H, 4 J_H and 8 C_H gene segments and of a distal 2.44-Mb-long V_H gene cluster containing 113 functional V_H genes[19,20]. D_H-J_H rearrangements occur in lymphoid progenitors followed by V_H gene recombination in pro-B-cells[16], which depends on *Igh* locus contraction to facilitate the participation of all V_H genes in V_H-DJ_H recombination[17,18,21]. D_H-J_H recombination[22] and rearrangements of the most 3' proximal V_H genes[23] depend on loop extrusion, explaining the

linear scanning activity of the RAG endonuclease, which ensures the orientation-biased cleavage of RSS elements in V(D)J recombination[24].

Cohesin is enriched in the genome at the DNA-bound zinc finger protein CTCF[25,26], which anchors chromatin loops by binding in an orientation-dependent manner to convergent CTCF-binding elements (CBEs)[4]. All 125 CBEs in the V_H gene cluster have the same directionality and are present in convergent orientation to one CBE in the IGCR1 region and 10 CBEs at the *Igh* 3' end (known as 3'CBEs)[20] (Extended Data Fig. 1a), suggesting that loops across the entire *Igh* locus may be formed by loop extrusion.

Results

Inverted *Igh* V_H genes do not recombine

To test the loop extrusion hypothesis, we inverted an 890-kb distal *Igh* region, containing 32 functional V_H genes and 49 CBEs that should be inefficient loop anchors, as they have the same reverse orientation as the 3'CBEs in the $Igh^{890\text{-inv}}$ allele (Extended Data Fig. 1b). While B-cell development was similar in $Igh^{890\text{-inv}/890\text{-inv}}$ and $Igh^{+/+}$ mice, the $Igh^{890\text{-inv}}$ allele in a competitive situation gave rise to half as many immature B-cells ($CD19^+B220^+IgM^+IgD^-$) as the wild-type allele in $Igh^{890\text{-inv}/+}$ mice (Extended Data Fig. 1c,d). Remarkably, the inverted V_H genes of the $Igh^{890\text{-inv}}$ allele were not expressed in immature B-cells (Extended Data Fig. 1e). Analysis of V(D)J recombination by VDJ-seq[27] revealed proportionally fewer VDJ_H-rearranged *Igh* alleles in bone marrow pro-B-cells ($CD19^+B220^+IgM^-IgD^-Kit^+CD25^-$) of $Igh^{890\text{-inv}/890\text{-inv}}$ mice compared to $Igh^{+/+}$ littermates (Extended Data Fig. 1f). The inverted V_H genes failed to undergo V_H-DJ_H recombination in $Igh^{890\text{-inv}/890\text{-inv}}$ pro-B-cells (Fig. 1a).

The lack of V_H-DJ_H recombination could be caused by the inverted CBEs preventing loop formation with the 3'CBEs, by inversion of the V_H genes or a combination of both. CTCF binding in the inverted region was normal in *Igh*$^{890\text{-inv}/890\text{-inv}}$ pro-B-cells (Extended Data Fig. 2a). As RAG2 deficiency prevents V(D)J recombination[16], we used *Igh*$^{890\text{-inv}/890\text{-inv}}$ *Rag2*$^{-/-}$ and *Igh*$^{+/+}$ *Rag2*$^{-/-}$ pro-B-cells for chromosome conformation capture sequencing (3C-seq) to map interactions from viewpoints at the *Igh* 5' or 3' end (Fig. 1b and Extended Data Fig. 2b,c). Interactions from the 3' viewpoint (HS5) to the inverted region (B) were 4.4-fold reduced in *Igh*$^{890\text{-inv}/890\text{-inv}}$ *Rag2*$^{-/-}$ pro-B-cells compared to *Igh*$^{+/+}$ *Rag2*$^{-/-}$ pro-B-cells (Fig. 1b,c and Extended Data Fig. 2c). Interactions from the 3' viewpoint to the 7 V_H genes at the *Igh* 5' end (A) were also decreased 3.2-fold in *Igh*$^{890\text{-inv}/890\text{-inv}}$ *Rag2*$^{-/-}$ pro-B-cells relative to *Igh*$^{+/+}$ *Rag2*$^{-/-}$ pro-B-cells (Fig. 1b,c), although these V_H genes with their 9 associated CBEs were present in normal forward orientation (Extended Data Fig. 1b). Recombination of 5 of these V_H genes (V_H1-80 to V_H1-84) in pro-B-cells and their subsequent expression in immature B-cells were strongly reduced (Fig. 1a and Extended Data Fig. 1e,g).

3C-seq analysis revealed a 1.5-fold increase of the interactions from the 5' viewpoint (V_H1-86) to the inverted region (B), but a 1.9-fold and 3-fold decrease of interactions to the middle (C) and 3' proximal (D) regions in *Igh*$^{890\text{-inv}/890\text{-inv}}$ *Rag2*$^{-/-}$ pro-B-cells compared to *Igh*$^{+/+}$ *Rag2*$^{-/-}$ pro-B-cells (Fig. 1b,c and Extended Data Fig. 2c). The inverted CBEs in region B thus interacted preferentially with the forward CBEs in region A on the *Igh*$^{890\text{-inv}}$ allele, which created a new loop domain in the distal V_H gene region (Extended Data Fig. 2d). Hence, the convergent orientation of the CBEs in the distal V_H gene cluster and the 3'CBEs promotes long-range interactions by loop extrusion across the entire *Igh* locus in wild-type pro-B-cells.

To study the effect of V_H gene inversion, we deleted the distal 890-kb region to generate the *Igh*$^{\Delta 890}$ allele, followed by re-insertion of the V_H8-8 gene with its 500-bp flanking sequences (lacking CBEs) in normal forward (*Igh*$^{V8\text{-}8}$) or inverted (*Igh*$^{V8\text{-}8\text{-}inv}$) orientation (Extended Data Fig. 2e and Supplementary Table 1b). mRNA expression of the inverted V_H8-8 gene was 9.4-fold reduced in immature *Igh*$^{V8\text{-}8\text{-}inv/\Delta 890}$ B-cells compared to *Igh*$^{V8\text{-}8/\Delta 890}$ B-cells (Extended Data Fig. 2f,g). VDJ-seq of *Igh*$^{V8\text{-}8\text{-}inv/V8\text{-}8\text{-}inv}$ and *Igh*$^{V8\text{-}8/V8\text{-}8}$ pro-B-cells demonstrated a 10.5-fold lower recombination frequency of the inverted V_H8-8 gene relative to the forward oriented V_H8-8 gene (Fig. 1d). This recombination frequency was still 3.6-fold higher in *Igh*$^{V8\text{-}8\text{-}inv/V8\text{-}8\text{-}inv}$ pro-B-cells compared to *Igh*$^{890\text{-}inv/890\text{-}inv}$ pro-B-cells (Fig. 1d), indicating that the recombination was further impaired upon inversion of the CBEs flanking the V_H8-8 gene in the *Igh*$^{890\text{-}inv}$ allele. In summary, efficient V_H-DJ_H recombination depends on the forward orientation of both the V_H genes and associated CTCF-binding sites.

Inverted CBEs impair V_H recombination

Loop extrusion across the *Igh* locus predicts that the insertion of multiple inverted CBEs (mimicking the 3'CBEs) in the V_H gene cluster may induce a new loop pattern interfering with distal V_H-DJ_H recombination. To test this, we generated the *Igh*$^{CBE\text{-}inv}$ and control *Igh*^{CBE} alleles by inserting an array of 20 CBEs in inverted or forward orientation in the middle of the *Igh* locus, respectively (Fig. 1e, Extended Data Fig. 3a and Supplementary Table 1c). The inserted arrays were efficiently bound by CTCF (Fig. 1e and Extended Data Fig. 3b). Expression of the V_H genes located upstream of the inverted CBE array in the *Igh*$^{CBE\text{-}inv}$ allele was strongly reduced in immature B-cells of *Igh*$^{CBE\text{-}inv/+}$ mice compared to the respective V_H genes of the

Igh^{CBE} allele in *Igh*$^{CBE/+}$ mice (Extended Data Fig. 3c,d). VDJ-seq demonstrated that the V_H genes, located 5' of the inverted CBE array up to the V_H1-61 gene at a distance of 355 kb, recombined at a significantly lower efficiency in *Igh*$^{CBE\text{-}inv/CBE\text{-}inv}$ pro-B-cells compared to *Igh*$^{CBE/CBE}$ pro-B-cells (Fig. 1f) or wild-type *Igh*$^{+/+}$ pro-B-cells (Extended Data Fig. 3e,f). 3C-seq revealed that the long-range interactions from the 3' viewpoint (HS5) to the V_H gene region A, located upstream of the inverted CBE array, were 1.7- or 1.9-fold decreased in *Igh*$^{CBE\text{-}inv/CBE\text{-}inv}$ pro-B-cells compared to *Igh*$^{CBE/CBE}$ or *Igh*$^{+/+}$ pro-B-cells, while the interactions to the downstream region B were 1.2- or 1.4-fold increased, respectively (Extended Data Fig. 4a,b,e). Conversely, the interactions from the 5' viewpoint (CBE), located immediately 5' of the CBE array insertion (Extended Data Fig. 2b and Supplementary Table 1c), to the upstream region A were 1.5- or 1.9-fold increased, and the interactions to the downstream region B were 1.4- or 1.6-fold decreased in *Igh*$^{CBE\text{-}inv/CBE\text{-}inv}$ pro-B-cells compared to the *Igh*$^{CBE/CBE}$ and *Igh*$^{+/+}$ pro-B-cells, respectively (Extended Data Fig. 4c,d,f). Hence, the insertion of a second 3'CBE-like element created a new loop domain in the distal V_H gene region of the *Igh*$^{CBE\text{-}inv}$ allele, which interfered with efficient loop formation from the *Igh* 3' end (Extended Data Fig. 4g). In summary, the analyses of the distal 890-kb inversion and inverted CBE array insertion together demonstrate that loop extrusion occurs across the *Igh* locus, generating extraordinarily long loops of up to a 2.8-Mb size.

Pax5 represses *Wapl* in precursor B-cells

As loop extrusion depends on cohesin[8-10], we investigated whether cohesin components are differentially expressed in pro-B-cells. mRNA expression of the cohesin-release factor Wapl[10,14,15] was down-regulated 4-fold only in pro-B and pre-B-cells within the lymphoid system

in contrast to other cohesin genes such as *Smc3* (Fig. 2a and Extended Data Fig. 5a). Wapl protein expression was similarly down-regulated in pro-B-cells compared to mature B-cells ($CD19^{+}B220^{+}IgD^{+}$; Extended Data Fig. 5b), indicating that the reduced Wapl expression may increase the residence time of cohesin on chromatin in pro-B-cells. To test this, we generated a *Smc3-Gfp* transgenic mouse expressing the Smc3-GFP protein in all cell types (Extended Data Fig. 5c). Smc3-GFP interacted with Smc1, Scc1 and Wapl (Extended Data Fig. 5d), suggesting that the fusion protein was functional. Bone marrow pro-B-cells and splenic mature B-cells of *Smc3-Gfp* transgenic mice were analysed by inverse fluorescence recovery after photobleaching (iFRAP; Extended Data Fig. 5e). The fluorescence signal recovered more slowly in $Wapl^{low}$ pro-B-cells compared to $Wapl^{high}$ mature B-cells (Fig. 2b), demonstrating that the residence time of cohesin on chromatin was increased in pro-B-cells consistent with extended loop extrusion creating long-range interactions across the *Igh* locus.

As Pax5 controls *Igh* locus contraction[17,18], we investigated whether Pax5 represses *Wapl* expression in pro-B-cells. *Wapl* mRNA was 4.1- or 5.9-fold more highly expressed in *ex vivo* sorted $Pax5^{-/-}$ or short-term cultured $Pax5^{\Delta/\Delta}$ (*Vav*-Cre $Pax5^{fl/fl}$) progenitors ($CD19^{-}B220^{+}Kit^{+}Ly6D^{+}$) compared to wild-type pro-B-cells (Fig. 2c). Wapl protein expression was similarly increased in $Pax5^{-/-}$ progenitors relative to $Rag2^{-/-}$ pro-B-cells (Fig. 2d). In pro-B-cells, Pax5 bound to two sites (P1 and P2) at the *Wapl* locus (Fig. 2e), with the P1 site being located in the $H3K4me3^{+}$ promoter at a distance of 310 bp from the transcription start site. Pax5 binding was, however, lost at the P1 site in mature B-cells (Fig. 2e). The *Wapl* promoter was present in open chromatin from multipotent progenitors (MPPs) to terminally differentiated plasmablasts, whereas open chromatin was detected at the P2 region only upon Pax5 expression (Extended Data Fig. 5f). Hence, the P1 and P2 sites may be involved in *Wapl* repression.

The Pax5 motif was unequivocally identified at the P1 site, but was less well defined at the P2 site (Extended Data Fig. 6a). We inactivated the P1 site by eliminating 10 bp of its Pax5 motif and deleted the P2 site by removing a 339-bp region by CRISPR/Cas9-mediated mutagenesis to generate the *Wapl*$^{\Delta P1,2}$ allele, which inadvertently resulted in a 5-bp deletion downstream of P1 (Extended Data Fig. 6a). Deletion of the P1 site prevented Pax5 binding to the *Wapl* promoter (Extended Data Fig. 6b). *Wapl* transcripts were increased 2.9- and 4.2-fold in *ex vivo* sorted *Wapl*$^{\Delta P1,2/\Delta P1,2}$ pro-B-cells and pre-B-cells (CD19^{+}B220^{+}IgM^{-}IgD^{-}Kit^{-}CD25^{+}) compared to *Wapl*$^{+/+}$ cells, respectively (Fig. 2f), while *Wapl* expression levels in heterozygous *Wapl*$^{\Delta P1,2/+}$ pro-B and pre-B-cells were between those of the homozygous and wild-type cells (Extended Data Fig. 6e). Increased *Wapl* mRNA and protein expression was confirmed in short-term cultured *Wapl*$^{\Delta P1,2/\Delta P1,2}$ pro-B-cells (Extended Data Fig. 6c,d). *Wapl* mRNA was, however, similarly expressed throughout T-cell development in *Wapl*$^{\Delta P1,2/\Delta P1,2}$ and *Wapl*$^{+/+}$ mice (Extended Data Fig. 6e), Hence, deletion of both P1 and P2 increased *Wapl* expression only in pro-B and pre-B-cells, identifying *Wapl* as a repressed Pax5 target gene in early B-cell development.

Wapl Pax5 site induces _Igh_ loop extrusion

B-cell development was strongly arrested at the pro-B-cell stage in the bone marrow of *Wapl*$^{\Delta P1,2/\Delta P1,2}$ and *Wapl*$^{\Delta P1,2/+}$ mice (Fig. 3a,b). We next generated the *Wapl*$^{\Delta P1}$ and *Wapl*$^{\Delta P2}$ alleles (Extended Data Fig. 6a). *Wapl* expression was increased in pro-B and pre-B-cells of *Wapl*$^{\Delta P1/+}$ and *Wapl*$^{\Delta P1/\Delta P1}$ mice, whereas it was similarly expressed in *Wapl*$^{\Delta P2/\Delta P2}$ and *Wapl*$^{+/+}$ pro-B-cells (Extended Data Fig. 7a,b). The pro-B-cell block was strong in *Wapl*$^{\Delta P1/\Delta P1}$

mice and slightly attenuated in *Wapl*$^{\Delta P1/+}$ mice (Fig. 3c,d), while B-cell development was normal in *Wapl*$^{\Delta P2/\Delta P2}$ mice (Extended Data Fig. 7c,d). Hence, the developmental block is caused by loss of a single Pax5-binding site in the *Wapl* promoter. Notably, pro-B-cells were lost upon conditional inactivation of *Wapl* in lymphoid progenitors of *Rag1*$^{Cre/+}$ *Wapl*$^{fl/fl}$ mice or in pro-B-cells of *Cd79a*$^{Cre/+}$ *Wapl*$^{fl/fl}$ mice (Extended Data Fig. 7e-g), indicating that pro-B-cells do not tolerate the complete loss of Wapl, while the physiological 4-fold down-regulation of Wapl expression in wild-type pro-B-cells promotes B-cell development.

VDJ-seq revealed that the proportion of VDJ_H-rearranged sequences was strongly reduced in pro-B-cells with the P1 site deletion (*Wapl*$^{\Delta P1,2/\Delta P1,2}$, *Wapl*$^{\Delta P1,2/+}$ and *Wapl*$^{\Delta P1/\Delta P1}$; Extended Data Fig. 8a). The middle and distal V_H genes failed to undergo V_H-DJ_H recombination in pro-B-cells with the P1 site deletion (*Wapl*$^{\Delta P1,2/\Delta P1,2}$, *Wapl*$^{\Delta P1,2/+}$ and *Wapl*$^{\Delta P1/\Delta P1}$) in contrast to their normal recombination in *Wapl*$^{\Delta P2/\Delta P2}$ and *Wapl*$^{+/+}$ pro-B-cells (Fig. 3e and Extended Data Fig. 8b). The recombination frequency of the proximal V_H genes declined with increasing distance from the 3' end of the V_H gene cluster, as the two most proximal functional V_H genes (V_H5-2 (V_H81X) and V_H2-2) rearranged at a higher frequency, the next three V_H genes (V_H5-4, V_H2-3 and V_H5-6) at a similar frequency and the following V_H genes started to lose their potential to undergo V_H-DJ_H recombination in *Wapl*$^{\Delta P1,2/\Delta P1,2}$, *Wapl*$^{\Delta P1,2/+}$ and *Wapl*$^{\Delta P1/\Delta P1}$ pro-B-cells (Fig. 3e). An equally strong recombination phenotype was observed in *Pax5*$^{\Delta/\Delta}$ progenitors (Fig. 3e), which are unable to contract the *Igh* locus[17,18]. Notably, *v-Abl* transformed pro-B-cells also do not undergo *Igh* locus contraction[23], as they express *Wapl* mRNA at the same high level as *Wapl*$^{\Delta P1,2/\Delta P1,2}$ pro-B-cells (Extended Data Fig. 8c).

3C-seq analysis of *Wapl*$^{\Delta P1,2/\Delta P1,2}$ *Rag2*$^{-/-}$ pro-B-cells demonstrated that interactions from the 3' viewpoint (HS5) were only observed over a 0.44-Mb-long region up to the most 3' proximal sequences of the V_H gene cluster (Fig. 3f), including the 5 V_H genes that could still undergo efficient V_H-DJ_H recombination in *Wapl*$^{\Delta P1,2/\Delta P1,2}$ pro-B-cells. Likewise, interactions from the 5' viewpoints (V_H1-83/81) could be detected only in the distal V_H gene region in *Wapl*$^{\Delta P1,2/\Delta P1,2}$ *Rag2*$^{-/-}$ pro-B-cells (Extended Data Fig. 8d), whereas interactions from both viewpoints extended across the 2.8-Mb-long *Igh* locus in *Rag2*$^{-/-}$ pro-B-cells (Figs. 1b and 3f). The low Wapl expression in wild-type pro-B-cells thus results in a 6-fold extension of the proximal interaction domain from 0.44 Mb to 2.8 Mb.

Pax5 recruits PRC2 to the *Wapl* promoter

Analysis of the chromatin landscape at the *Wapl* locus revealed that the active histone mark H3K4me3 was abundantly present at the *Wapl* promoter in Pax5-deficient progenitors and Pax5-expressing control pro-B-cells (Fig. 4a). In contrast, the repressive histone mark H3K27me3, which is produced by the Polycomb repressive complex 2 (PRC2) consisting of the core components Eed, Ezh2 and Suz12 (ref. 28), was detected at the *Wapl* promoter only in Pax5-expressing pro-B-cells, consistent with selective binding of Ezh2 and Suz12 in these cells (Fig. 4a). We generated a floxed *Eed*^{fl} allele (Extended Data Fig. 9a) for elimination of this essential PRC2 component in pro-B-cells of *Rag1*$^{Cre/+}$ *Eed*$^{fl/fl}$ mice. In Eed-deficient pro-B-cells, H3K27me3 was absent at the *Wapl* promoter in contrast to its residual presence at other locations in the locus (Fig. 4b). Moreover, H3K27me3 was specifically lost at the *Wapl* promoter in *Wapl*$^{\Delta P1/\Delta P1}$ pro-B-cells (Fig. 4b and Extended Data Fig. 9b), and Ezh2 (PRC2) binding was absent upon loss of Pax5 binding at the P1 site in mature B-cells (Extended Data Fig. 9c). Hence,

Pax5 may recruit PRC2 to the P1 site in early B-lymphopoiesis. To investigate this, we performed streptavidin-pulldown experiments with nuclear extracts prepared from HEK-293T cells that were transiently transfected with expression vectors encoding Pax5-Bio-IRES-BirA and Myc-tagged Ezh2 or IRF4 proteins. Streptavidin-pulldown of Pax5-Bio specifically co-precipitated Myc-Ezh2 but not Myc-IRF4 (Extended Data Fig. 9d). We conclude that Pax5-mediated recruitment of PRC2 represses the *Wapl* promoter by inducing bivalent chromatin ($H3K4me3^{+}$ $H3K27me3^{+}$) in pro-B-cells.

B-cell development in *Rag1*$^{Cre/+}$ *Eed*$^{fl/fl}$ mice was stringently blocked at pro-B-cells, which exhibited impaired activation of 93 genes and de-repression of 430 genes including *Cdkn2a* and *Cdkn2b* encoding cell cycle inhibitors (Extended Data Fig. 9e-g and Supplementary Table 2). However, genes encoding cohesin subunits and key regulators of early B-cell development were similarly expressed in Eed-deficient and control pro-B-cells (Extended Data Fig. 9h). In contrast, *Wapl* expression was derepressed 3-fold in *Rag1*$^{Cre/+}$ *Eed*$^{fl/fl}$ pro-B-cells and 4.2-fold in *Rag1*$^{Cre/+}$ *Eed*$^{fl/fl}$ *Cdkn2ab*$^{-/-}$ pro-B-cells (Fig. 4c). Consequently, V_H-DJ_H recombination in Eed-deficient pro-B-cells was strongly reduced and was only observed for the most 3' proximal V_H genes (Fig. 4d and Extended Data Fig. 9i,j), similar to *Pax5*$^{\Delta/\Delta}$ progenitors and pro-B-cells lacking the *Wapl* P1 site (Fig. 3e). In summary, Pax5 recruits PRC2 to the *Wapl* promoter to induce bivalent chromatin, which leads to down-regulation of *Wapl* expression, extension of loop extrusion across the *Igh* locus and thus participation of all V_H genes in V_H-DJ_H recombination.

Pax5 sculpts the chromosomal architecture

To investigate whether *Wapl* repression by Pax5 induces global chromosomal changes in pro-B-cells, we performed iFRAP experiments with mutant and wild-type pro-B and mature B-cells

expressing the *Smc3-Gfp* transgene. Recovery of the fluorescence signal after photobleaching was slow only in *Wapl*$^{+/+}$ pro-B-cells compared to the faster recovery observed with *Pax5*$^{-/-}$ progenitors and *Wapl*$^{\Delta P1,2/+}$ pro-B-cells (Fig. 5a) as well as *Wapl*$^{\Delta P1,2/+}$ and *Wapl*$^{+/+}$ mature B-cells (Extended Data Fig. 10a). Hence, Pax5 controls the residence time of cohesin on chromatin only in early B-cell development, consistent with the loss of Pax5 and Ezh2 binding at the *Wapl* promoter in mature B-cells (Fig. 2e and Extended Data Fig. 9c).

We next studied the genome-wide chromosomal architecture of pro-B and mature B-cells by *in situ* Hi-C[4]. Analysis of all identified sequence contacts revealed that the frequencies of contacts up to a distance of 5 Mb, which largely generate chromatin loops within TADs[4], were significantly lower in *Pax5*$^{\Delta/\Delta}$ progenitors, *Wapl*$^{\Delta P1,2/\Delta P1,2}$ pro-B-cells and *Wapl*$^{+/+}$ mature B-cells compared to *Wapl*$^{+/+}$ pro-B-cells (Fig. 5b and Extended Data Fig. 10b). In contrast, the frequencies of contacts over very large distances (> 10 Mb), which mainly give rise to chromosomal compartments[1], were strongly increased in *Pax5*$^{\Delta/\Delta}$ progenitors, *Wapl*$^{\Delta P1,2/\Delta P1,2}$ pro-B-cells and *Wapl*$^{+/+}$ mature B-cells relative to *Wapl*$^{+/+}$ pro-B-cells (Fig. 5b and Extended Data Fig. 10b). Consequently, the Hi-C contact map of chromosome 12 revealed a better-defined 'checkerboard' pattern of higher intensity for *Pax5*$^{\Delta/\Delta}$ progenitors, *Wapl*$^{\Delta P1,2/\Delta P1,2}$ pro-B-cells and *Wapl*$^{+/+}$ mature B-cells compared to *Wapl*$^{+/+}$ pro-B-cells (Fig. 5c). Hi-C contact maps of zoomed-in regions on chromosomes 12 and 16 demonstrated a significant extension of loops in *Wapl*$^{+/+}$ pro-B-cells compared to *Pax5*$^{\Delta/\Delta}$ progenitors and *Wapl*$^{\Delta P1,2/\Delta P1,2}$ pro-B-cells (Extended Data Fig. 10c). The number of loops was increased by a factor of 1.9 and 1.6 and the average loop length by a factor of 1.5 and 2.2 in *Wapl*$^{+/+}$ pro-B-cells compared to *Pax5*$^{\Delta/\Delta}$ progenitors and *Wapl*$^{\Delta P1,2/\Delta P1,2}$ pro-B-cells, respectively (Fig. 5d,e and Extended Data Fig.

10d). The Hi-C contact map of the *Igh* locus confirmed the 3C-seq results, as loops across the entire *Igh* locus were seen in *Wapl*$^{+/+}$ pro-B-cells in contrast to *Wapl*$^{\Delta P1,2/\Delta P1,2}$ pro-B-cells (Fig. 5f). Only a relatively small number of genes was upregulated (161) or downregulated (159) in *Wapl*$^{\Delta P1,2/\Delta P1,2}$ pro-B-cells relative to *Wapl*$^{+/+}$ pro-B-cells (Extended Data Fig. 10e,f and Supplementary Table 3). Genes coding for key regulators of early B-cell development or cohesin subunits other than Wapl were not deregulated (Extended Data Fig. 10g). In summary, the 4-fold repression of *Wapl*, mediated by a single Pax5-binding site (P1), leads to massive alterations of the chromosomal architecture in pro-B-cells.

Discussion

The long-range interaction and V_H-DJ_H recombination defects, observed upon inversion of a distal 890-kb region or insertion of an inverted CBE array in the *Igh* locus, provide strong evidence that it is the loop extrusion mechanism rather than any other folding principle that creates the long-range interactions across the *Igh* locus. The finding that a distal V_H gene upon its inversion can no longer participate in V_H-DJ_H recombination demonstrates an essential role for loop extrusion in correctly positioning the convergent RSS elements of the V_H and DJ_H-rearranged gene segments for RAG-mediated cleavage and recombination[16]. In a 'stable' loop anchored at the 3'CBEs, the RSS elements of two adjacent gene segments could be correctly aligned by local diffusion (Extended Data Fig. 10h). However, as loop extrusion may initiate at any position within the *Igh* locus, it is also conceivable that cohesin rings moving by symmetrical loop extrusion[11,12] through the RAG-bound recombination centre[29] may correctly position the RSS sequences of a V_H gene and the DJ_H-rearranged gene segment for subsequent RAG-mediated cleavage (Extended Data Fig. 10i). This model of correct RSS alignment through

ongoing loop extrusion could also explain why an inverted V_H gene cannot rearrange due to misalignment of the respective RSS elements (Extended Data Fig. 10j).

The 4-fold repression of *Wapl* by Pax5 causes global changes of the chromosomal architecture in pro-B-cells, as the number and length of chromatin loops are significantly increased, while the compartments are weakened similar to observations made with Wapl-depleted human cell lines[10,15]. This global phenotype is exquisitely sensitive to small changes of Wapl expression, as a 2-fold increase of *Wapl* expression in *Wapl*$^{\Delta P1,2/+}$ pro-B-cells is sufficient to decrease the residence time of cohesin on chromatin, to abolish long-range looping across the *Igh* locus and, by inference, to induce global alterations in the chromosome architecture. In summary, the entire genome of pro-B-cells undergoes massive three-dimensional changes to facilitate the generation of a diverse antibody repertoire through participation of all V_H genes in V_H-DJ_H recombination, which depends on prolonged loop extrusion across the *Igh* locus.

Online content

Any methods, additional references, Nature Research reporting summaries, source data, extended data, supplementary information, acknowledgements; details of author contributions and competing interests; and statement of data availability are available at https: xyz.

References

1. Lieberman-Aiden, E. *et al.* Comprehensive mapping of long-range interactions reveals folding principles of the human genome. *Science* **326**, 289-293 (2009).
2. Dixon, J. R. *et al.* Topological domains in mammalian genomes identified by analysis of chromatin interactions. *Nature* **485**, 376-380 (2012).
3. Nora, E. P. *et al.* Spatial partitioning of the regulatory landscape of the X-inactivation centre. *Nature* **485**, 381-385 (2012).

4. Rao, S. S. *et al.* A 3D map of the human genome at kilobase resolution reveals principles of chromatin looping. *Cell* **159**, 1665-1680 (2014).
5. Nasmyth, K. Disseminating the genome: joining, resolving, and separating sister chromatids during mitosis and meiosis. *Annu. Rev. Genet.* **35**, 673-745 (2001).
6. Sanborn, A. L. *et al.* Chromatin extrusion explains key features of loop and domain formation in wild-type and engineered genomes. *Proc. Natl. Acad. Sci. USA* **112**, E6456-E6465 (2015).
7. Fudenberg, G. *et al.* Formation of chromosomal domains by loop extrusion. *Cell reports* **15**, 2038-2049 (2016).
8. Rao, S. S. P. *et al.* Cohesin loss eliminates all loop domains. *Cell* **171**, 305-320 (2017).
9. Schwarzer, W. *et al.* Two independent modes of chromatin organization revealed by cohesin removal. *Nature* **551**, 51-56 (2017).
10. Wutz, G. *et al.* Topologically associating domains and chromatin loops depend on cohesin and are regulated by CTCF, WAPL, and PDS5 proteins. *EMBO J.* **36**, 3573-3599 (2017).
11. Davidson, I. F. *et al.* DNA loop extrusion by human cohesin. *Science* **366**, 1338-1345 (2019).
12. Kim, Y., Shi, Z., Zhang, H., Finkelstein, I. J. & Yu, H. Human cohesin compacts DNA by loop extrusion. *Science* **366**, 1345-1349 (2019).
13. Kueng, S. *et al.* Wapl controls the dynamic association of cohesin with chromatin. *Cell* **127**, 955-967 (2006).
14. Tedeschi, A. *et al.* Wapl is an essential regulator of chromatin structure and chromosome segregation. *Nature* **501**, 564-568 (2013).
15. Haarhuis, J. H. I. *et al.* The cohesin release factor WAPL restricts chromatin loop extension. *Cell* **169**, 693-707 (2017).
16. Alt, F. W., Zhang, Y., Meng, F.-L., Guo, C. & Schwer, B. Mechanisms of programmed DNA lesions and genomic instability in the immune system. *Cell* **152**, 417-429 (2013).
17. Fuxa, M. *et al.* Pax5 induces *V*-to-*DJ* rearrangements and locus contraction of the *immunoglobulin heavy-chain* gene. *Genes Dev.* **18**, 411-422 (2004).
18. Medvedovic, J. *et al.* Flexible long-range loops in the V_H gene region of the *Igh* locus facilitate the generation of a diverse antibody repertoire. *Immunity* **39**, 229-244 (2013).
19. Johnston, C. M., Wood, A. L., Bolland, D. J. & Corcoran, A. E. Complete sequence assembly and characterization of the C57BL/6 mouse Ig heavy chain V region. *J. Immunol.* **176**, 4221-4234 (2006).

20. Proudhon, C., Hao, B., Raviram, R., Chaumeil, J. & Skok, J. A. Long-range regulation of V(D)J recombination. *Adv. Immunol.* **128**, 123-182 (2015).
21. Jhunjhunwala, S. *et al.* The 3D structure of the immunoglobulin heavy-chain locus: implications for long-range genomic interactions. *Cell* **133**, 265-279 (2008).
22. Zhang, Y. *et al.* The fundamental role of chromatin loop extrusion in physiological V(D)J recombination. *Nature* **573**, 600-604 (2019).
23. Jain, S., Ba, Z., Zhang, Y., Dai, H. Q. & Alt, F. W. CTCF-binding elements mediate accessibility of RAG substrates during chromatin scanning. *Cell* **174**, 102-116 (2018).
24. Hu, J. *et al.* Chromosomal loop domains direct the recombination of antigen receptor genes. *Cell* **163**, 947-959 (2015).
25. Parelho, V. *et al.* Cohesins functionally associate with CTCF on mammalian chromosome arms. *Cell* **132**, 422-433 (2008).
26. Wendt, K. S. *et al.* Cohesin mediates transcriptional insulation by CCCTC-binding factor. *Nature* **451**, 796-801 (2008).
27. Chovanec, P. *et al.* Unbiased quantification of immunoglobulin diversity at the DNA level with VDJ-seq. *Nat. Protoc.* **13**, 1232-1252 (2018).
28. Margueron, R. & Reinberg, D. The Polycomb complex PRC2 and its mark in life. *Nature* **469**, 343-349 (2011).
29. Ji, Y. *et al.* The in vivo pattern of binding of RAG1 and RAG2 to antigen receptor loci. *Cell* **141**, 419-431 (2010).
30. Durand, N. C. *et al.* Juicer provides a one-click system for analyzing loop-resolution Hi-C experiments. *Cell Syst.* **3**, 95-98 (2016).

Figure legends

Fig. 1 | Inversion of an 890-kb *Igh* region and insertion of inverted CBEs interfere with V_H gene recombination. a, VDJ-seq analysis[27] of *Igh*$^{890\text{-inv}/890\text{-inv}}$ bone marrow pro-B-cells. V_H gene usage is shown as mean percentage (with SEM) of all VDJ_H recombination events in *Igh*$^{+/+}$ or *Igh*$^{890\text{-inv}/890\text{-inv}}$ pro-B-cells. The V_H genes (Supplementary Table 1a) are aligned according to their *Igh* position. **b**, 3C-seq analysis of interactions from a 3' viewpoint (HS5) or 5'

viewpoint (V_H1-86) in short-term cultured *Igh*$^{890\text{-inv}/890\text{-inv}}$ *Rag2*$^{-/-}$ and *Igh*$^{+/+}$ *Rag2*$^{-/-}$ pro-B-cells. Normalized counts of the 3C-seq reads are plotted. One of two 3C-seq experiments is shown. **c**, Quantification of interactions. The 3C-seq reads in regions A-D (**b**) were quantified as mean RPM value per region for each viewpoint. RPM, reads per million mapped sequence reads. **d**, VDJ-seq analysis of the V_H8-8 recombination frequency in pro-B-cells of the indicated genotypes. **e**, CTCF binding at an array of 20 CBEs, inserted at position 116,242,836 (mm9, chromosome 12) in forward (*Igh*$^{\text{CBE /CBE}}$) or reverse (*Igh*$^{\text{CBE-inv/CBE-inv}}$) orientation, as determined by ChIP-seq (Extended Data Fig. 3b). **f**, VDJ-seq analysis of V_H gene recombination at the *Igh* 5' end in *Igh*$^{\text{CBE/CBE}}$ and *Igh*$^{\text{CBE-inv/CBE-inv}}$ pro-B-cells. Statistical data in **d** were analysed by one-way ANOVA with Tukey's post-hoc test. *n*, number of experiments. Each dot corresponds to one mouse (**c**,**d**).

Fig. 2 | Pax5-dependent repression of *Wapl* in pro-B and pre-B-cells.

a, Expression of *Wapl* and *Smc3* in developing B-cells. RNA-seq expression data for the indicated cell types (Methods) are shown as mean TPM values with SEM. LMPP, lymphoid-primed multipotent progenitors; ALP, all-lymphoid progenitors; BLP, B-cell-biased lymphoid progenitors; FO and GC B, follicular and germinal centre B-cells; PC, plasma cells. For experiment numbers see source data. **b**, iFRAP analysis of short-term cultured bone marrow pro-B-cells and *ex vivo* sorted splenic mature B-cells from *Smc3-Gfp* transgenic mice. The difference in fluorescence intensity between bleached and unbleached regions is plotted against time. The mean values are indicated by lines and the SD by shading. *n*, number of cells analysed. **c**, *Wapl* expression in *ex vivo* sorted and *in vitro* cultured pro-B-cells of the indicated genotypes. **d**, Wapl expression in cultured *Pax5*$^{-/-}$ progenitors and *Rag2*$^{-/-}$ pro-B-cells, determined by immunoblotting of whole-cell extracts with antibodies detecting Wapl, Pax5 or TBP. One of two

experiments is shown with marker proteins (kilodaltons). **e**, Detection of Pax5 binding and H3K4me3 at the *Wapl* locus in bone marrow pro-B-cells and splenic mature B-cells by ChIP-seq. The Pax5 peaks P1 and P2 are indicated. One of two experiments is shown. **f**, *Wapl* expression in pro-B and pre-B-cells of *Wapl*$^{\Delta P1,2/\Delta P1,2}$ and *Wapl*$^{+/+}$ mice is shown as mean TPM values. *n*, number of RNA-seq experiments (**c**,**f**).

Fig. 3 | The Pax5-binding site at the *Wapl* promoter controls loop extrusion and V_H-DJ_H recombination. a-d, Flow cytometric analysis of B-cell development in the bone marrow of the indicated genotypes. The percentage of pro-B and pre-B-cells is indicated for one of five experiments (**a**,**c**), and the relative frequencies of the indicated cell types are shown as mean values with SEM (**b**,**d**). **e**, V_H gene recombination in *Wapl*$^{+/+}$ and mutant pro-B-cells, determined by pairwise VDJ-seq experiments. The VDJ-seq data of *Wapl*$^{+/+}$ and mutant pro-B-cells are shown in the upper and lower part, respectively. The V_H gene usage is shown as mean percentage of all DJ_H and VDJ_H rearrangement events with SEM. **f**, 3C-seq analysis of interactions from the 3' viewpoint (HS5) in *Wapl*$^{\Delta P1,2/\Delta P1,2}$ *Rag2*$^{-/-}$ and *Wapl*$^{+/+}$ *Rag2*$^{-/-}$ pro-B-cells. The 0.44-Mb proximal loop domain and the position of the V_H5-6 gene are indicated. One of two 3C-seq experiments is shown. Statistical data in **b** and **d** were analysed by multiple *t*-tests (unpaired and two-tailed with Holm-Sidak correction); $^{**}P < 0.01$; $^{***}P < 0.001$; $^{****}P < 0.0001$. *n*, number of mice (**b**,**d**) or experiments (**e**). Each dot (**b**,**d**) corresponds to one mouse.

Fig. 4 | Pax5-mediated recruitment of PRC2 to the *Wapl* promoter facilitates V_H-DJ_H recombination. a, Epigenetic landscape at the *Wapl* locus in Pax5-deficient progenitors and Pax5-expressing control pro-B-cells. Binding of Pax5, Ezh2 and Suz12 and the presence of H3K4me3 and H3K27me3 were determined by ChIP-seq. One of two experiments per genotype

and antibody is shown. **b**, Selective loss of H3K27me3 at the *Wapl* promoter in *Rag1*$^{Cre/+}$ *Eed*$^{fl/fl}$ and *Wapl*$^{\Delta P1/\Delta P1}$ pro-B-cells. One of two experiments per genotype is shown. **c**, *Wapl* mRNA expression in *ex vivo* sorted pro-B-cells from mice of the indicated genotypes, as shown by mean TPM values. The *P* value and SEM (**c**, top) were determined by DESeq2. **d**, VDJ-seq analysis of pro-B-cells from *Rag1*$^{Cre/+}$ *Eed*$^{fl/fl}$ or control mice. The V_H gene usage is shown as mean percentage of all VDJ_H rearrangement events with SEM. *n*, number of experiments.

Fig. 5 | Pax5-dependent changes of the entire chromatin architecture in pro-B-cells. **a**, iFRAP analysis of short-term cultured bone marrow pro-B-cells from *Wapl*$^{\Delta P1,2/+}$, *Pax5*$^{-/-}$ and wild-type mice carrying the *Smc3-Gfp* transgene, as described in Fig. 2b. *n*, number of cells analysed. **b**, Frequency distribution of intra-chromosomal contacts as a function of the genomic distance using logarithmically increased genomic distance bins, as determined by HOMER analysis of Hi-C data generated with short-term cultured *Pax5*$^{\Delta/\Delta}$ progenitors, *Wapl*$^{+/+}$ pro-B-cells and *Wapl*$^{\Delta P1,2/\Delta P1,2}$ pro-B-cells. **c**, Hi-C contact matrices of chromosome 12 determined for *Pax5*$^{\Delta/\Delta}$ progenitors, *Wapl*$^{+/+}$ and *Wapl*$^{\Delta P1,2/\Delta P1,2}$ pro-B-cells and *ex vivo* sorted *Wapl*$^{+/+}$ mature B-cells, plotted at 250-kb bin resolution with Juicebox[30]. The intensity of each pixel represents the normalized number of contacts between a pair of loci[4] with the maximum intensity being indicated in the lower left corner. **d**, Number of chromatin loops (with a length of < 5 Mb) identified in *Pax5*$^{\Delta/\Delta}$ progenitors, *Wapl*$^{+/+}$ and *Wapl*$^{\Delta P1,2/\Delta P1,2}$ pro-B-cells with HiCCUPS[30]. **e**, Distribution of the loop length. The median (white lines), middle 50% of the data (boxes) and all values of 1.5× interquartile range (whiskers) are shown. **f**, Hi-C contact matrices of the *Igh* region. Black dots indicate loop anchors. Two Hi-C experiments per genotype were performed except for mature B-cells (one experiment).

Methods

Mice

The following mice were maintained on the C57BL/6 background: *Pax5*$^{+/-}$ mice[31], *Pax5*$^{fl/fl}$ mice[32], *Pax5*$^{Bio/Bio}$ mice[33], *Pax5*$^{ihCd2/ihCd2}$ mice[34], *Rag2*$^{-/-}$ mice[35], *Cdkn2ab*$^{+/-}$ mice[36], *Wapl*$^{fl/fl}$ mice[14], *Meox2*$^{Cre/+}$ mice[37], *Rag1*$^{Cre/+}$ mice[38], *Cd79a*(Mb1)$^{Cre/+}$ mouse[39], *Rosa26*$^{CreERt2/+}$ mice[40], transgenic *Vav*-Cre mice[41], transgenic Flpe mice[42] and transgenic CAGGs-Dre mice[43]. All animal experiments were carried out according to valid project licenses, which were approved and regularly controlled by the Austrian Veterinary Authorities.

Generation of mutant mice

Genetic alterations were introduced into the C57BL/6 *Igh* allele. The hybrid C57BL/6 × 129Sv ES cell line A9 was used for homologous recombination in ES cells. The *frt*-flanked *Pgk1-Neo* or *Pgk1-Puro* expression cassette, which was used for selection of the targeted ES cell clones, was deleted after germline transmission in the mutant mice additionally expressing the Flpe transgene[42], except for the generation of *Igh*$^{fl\text{-}890\text{-}fl}$ and *Igh*$^{ifl\text{-}890\text{-}fl}$ alleles. All mutant strains were back-crossed to the C57BL/6 background. The *Igh*$^{fl\text{-}890\text{-}fl}$ and *Igh*$^{ifl\text{-}890\text{-}fl}$ alleles were created by first inserting a *loxP* (fl) site at position 116,237,220 (mm9, Chr. 12) into the middle of the V_H gene cluster followed by insertion of a second *lox* (*lox*71) site (in the same orientation; *Igh*$^{fl\text{-}890\text{-}fl}$) or an inverted *lox*71 (ifl) site (*Igh*$^{ifl\text{-}890\text{-}fl}$) at position 117,126,667 in the *Igh* 5' region by ES cell targeting (Extended Data Fig. 1b). The *Igh*$^{890\text{-}inv}$ allele was generated by Cre-mediated inversion of the *lox*71/*lox*P-flanked *Igh* region in *Meox2*$^{Cre/+}$ *Igh*$^{ifl\text{-}890\text{-}fl/+}$ mice

(Extended Data Fig. 1b). The *Igh*$^{\Delta 890}$ allele was created by Cre-mediated deletion of the *lox*71/*lox*P-flanked *Igh* region in *Meox2*$^{Cre/+}$ *Igh*$^{fl\text{-}890\text{-}fl/+}$ mice. The *Igh*$^{V8\text{-}8}$ and *Igh*$^{V8\text{-}8\text{-}inv}$ alleles were generated by using the Floxin method[44] to insert the V_H8-8 gene in both orientations into *Igh*$^{\Delta 890/+}$ ES cells (Extended Data Fig. 2e and Supplementary Table 1b). The *rox*-flanked *Actb*-Bsd expression cassette, used for selection of targeted ES cells, was deleted after germline transmission with the CAGGs-Dre transgene, which left only one *frt* and one *rox* site in the targeted *Igh* locus. An array of 20 CBEs (Supplementary Table 1c) was inserted in both orientations at position 116,242,836 (mm9, Chr. 12) into the *Igh* locus by targeting *Rosa26*$^{CreERt2/+}$ ES cells to generate the *Igh*^{CBE} and *Igh*$^{CBE\text{-}inv}$ alleles (Extended Data Fig. 3a). The *lox*P-flanked *Pgk1-Neo* expression cassette, used for selection of targeted *Rosa26*$^{CreERt2/+}$ ES cells, was deleted by 4-hydroxytamoxifen-mediated induction of Cre activity in ES cells. The *Eed*^{fl} allele was created by ES cell targeting as described in detail in Extended Data Fig. 9a. The *Wapl*$^{\Delta P1,2/+}$, *Wapl*$^{\Delta P1/+}$ and *Wapl*$^{\Delta P2/+}$ mice were generated by CRISPR/Cas9-mediated genome editing in mouse zygotes[45] (C57BL/6 × CBA). For this, mouse zygotes were injected with Cas9 mRNA, a P1-specific sgRNA (linked to the scaffold tracrRNA) and a repair template to specifically delete the Pax5-binding site P1 and/or with Cas9 mRNA and two different P2-specific sgRNAs and a repair template to delete a 340-bp fragment encompassing the site P2 (Extended Data Fig. 6a and Supplementary Table 4). The *Smc3-Gfp* transgenic mouse line 43 was generated by injecting the pronucleus of a mouse zygote with the bacterial artificial chromosome (BAC) RP24-276L14 containing the *Smc3* locus that was modified by insertion of a C-terminal localization-affinity purification (LAP) tag comprising the green fluorescent protein (GFP)[46].

Antibodies

The following monoclonal antibodies were used for flow cytometric analysis of the mouse bone marrow, spleen and thymus: B220/CD45R (RA3-6B2), CD2 (RM2-5), CD3 (145-2C11), CD4 (L3T4), CD5 (53-7.3), CD8a (53-6.7), CD11b (M1/70), CD19 (1D3), CD21/CD35 (7G6), CD23 (B3B4), CD25/IL-2Rα (PC61), CD28 (37.51), CD44 (IM7), CD90.2/Thy1.2 (30-H12), CD95/Fas ((Jo2), CD115/MCSF-R (AFS98), CD117/Kit (2B8), CD127/IL-7Rα (A7R34), CD135/Flt3 (A2F10.1), CD138 (281-2), GL7(GL7), Gr1 (RB6-8C5), hCD2 (RPA-2.10), IgD (11-26c), IgM (II/41), IgM^a (MA-69), IgM^b (AF6-78), Ly6D (49H4), Sca1/Ly6A (D7), TCRβ (H57-597) and Ter119 (TER119).

The following antibodies were used for immunoblot or immunoprecipitation analyses: anti-Ezh2 (rabbit mAb clone D2C9; Cell Signaling) or anti-Ezh2 (rabbit polyclonal Ab, pAb-039-050; Diagenode), anti-Myc (mouse mAb clone 9E10; produced in-house), anti-Suz12 (rabbit mAb clone D39F6; Cell Signaling), anti-Pax5 (rabbit polyclonal Ab, detecting the paired domain (amino acids 17-145)[47]; Busslinger laboratory), anti-CTCF (rabbit polyclonal Ab 07-729; Merck Millipore), anti-Wapl (rabbit polyclonal Ab, A960; Peters laboratory), anti-TBP (mouse mAb clone 3TF1-3G3; Active Motif), anti-GFP (chicken polyclonal Ab, ab13970; Abcam), anti-Smc1 (rabbit polyclonal Ab, A300-055A; Bethyl Laboratories), anti-Smc3 (rabbit polyclonal Ab, A300-060A; Bethyl Laboratories), anti-Smc3ac (mouse mAb; a gift from K. Shirahige), anti-Scc1(Rad21) (mouse mAb 53A303; EMD Millipore Corporation), anti-Pds5a (rabbit polyclonal Ab, A300-089A; Bethyl Laboratories), anti-Pds5b (rabbit polyclonal Ab, A300-537A; Bethyl Laboratories), anti-H3K4me3 (rabbit polyclonal Ab, pAb-003-050; Diagenode) and anti-H3K27me3 (rabbit mAb 9733; Cell Signaling).

Definition of cell types by flow cytometry

Cell types were defined as follows in the bone marrow: MPP ($Lin^{-}Kit^{hi}Sca1^{hi}$), LMPP ($Lin^{-}Kit^{hi}Sca1^{hi}CD135^{+}$), ALP ($Lin^{-}CD127^{+}CD135^{+}Ly6D^{-}$), $Pax5^{-}$ BLP ($Lin^{-}CD127^{+}CD135^{+}Ly6D^{+}hCD2(Pax5)^{-}$), $Pax5^{+}$ BLP ($Lin^{-}CD127^{+}CD135^{+}Ly6D^{+}hCD2(Pax5)^{+}$), Pax5-deficient progenitors ($CD19^{-}B220^{+}Kit^{+}Ly6D^{+}$), pro-B cells ($CD19^{+}B220^{+}IgM^{-}IgD^{-}Kit^{+}CD25^{-}$), pre-B cells ($CD19^{+}B220^{+}IgM^{-}IgD^{-}Kit^{-}CD25^{+}$), immature B cells ($CD19^{+}B220^{+}IgM^{+}IgD^{-}$), recirculating B cells ($CD19^{+}B220^{+}IgD^{+}$), plasma cells $Lin^{-}GFP(Blimp1)^{hi}B220^{lo}CD138^{hi}CD28^{+}$, macrophages ($CD115^{+}Gr1^{int}$), granulocytes ($Gr1^{+}$); in the spleen: immature B cells ($CD19^{+}B220^{+}IgM^{+}IgD^{-}$), mature B cells ($CD19^{+}B220^{+}IgD^{+}$), follicular (FO) B cells ($CD19^{+}B220^{+}CD23^{+}CD21^{lo}$), germinal centre (GC) B cells ($CD19^{+}B220^{+}GL7^{+}Fas^{+}$), T cells ($TCR\beta^{+}$), $CD4^{+}$ T cells ($CD4^{+}CD8^{-}$), $CD8^{+}$ T cells ($CD4^{-}CD8^{+}$); in the thymus: DN T cells ($CD4^{-}CD8^{-}CD90.2^{+}$), DP T cells ($CD4^{+}CD8^{+}$), $CD4^{+}$ SP T cells ($CD4^{+}CD8^{-}$), $CD8^{+}$ SP T cells ($CD4^{-}CD8^{+}$). Lineage depletion (Lin^{-}) was performed using the MagniSort™ Mouse Hematopoietic Lineage Depletion Kit (Thermo Fisher Scientific), which contains anti-CD2, CD3, CD5, CD11b, CD19, B220/CD45R, Ly6G and Ter119 antibodies. Flow cytometry experiments and FACS sorting were performed on LSR Fortessa (BD Biosciences) and FACSAria III (BD Biosciences) machines, respectively. Flowjo software (Treestar) was used for data analysis.

***In vitro* culture of pro-B cells**

Pro-B cells and Pax5-deficient progenitors were cultured on OP9 cells in IL-7-containing IMDM as described[48].

RT-qPCR analysis of mRNA expression

Total RNA was prepared from distinct B and T cell types sorted from the bone marrow, thymus and spleen or from *in vitro* cultured *v-Abl* pro-B cell lines, using a semi-automated RNA bead isolation method with Sera-Mag SpeedBead Carboxylate-Modified Magnetic Particles (Hydrophobic; GE Healthcare) run on the magnetic particle processor KingFisher Duo instrument (Thermo Fisher Scientific). The cDNA was synthesized using Oligo $d(T)_{18}$ primer (NEB) and SuperScript® II Reverse Transcriptase (Thermo Fisher Scientific) in the presence of RNase inhibitor (Thermo Fisher Scientific). The transcripts of selected genes were amplified by qPCR using primers located in different exons (Supplementary Table 4) and were normalized against the *Tbp* mRNA.

Transient transfection and co-precipitation analysis

To investigate the interaction of Pax5-Bio with PRC2 by co-precipitation experiments (Extended Data Fig. 9d), 1.5×10^7 HEK-293T cells were transiently transfected by Lipofectamine (Invitrogen) with the expression plasmids pCMV-mPax5-Bio-IRES-BirA (1 μg), pCMV-myc-hEzh2 (1 μg), pCMV-hSuz12 (1 μg) and pCMV-mEed (1μg) or with pCMV-mPax5-Bio-IRES-BirA (1 μg) and pCMV-myc-mIRF4 (1 μg). Two days after transfection, nuclear extracts were prepared as described in detail[49] and their protein content was measured by Bradford assay (BioRad). All Dynabeads used for streptavidin pulldown were incubated with 1 mg/ml BSA in PBS overnight at 4 °C. Nuclear extracts were precleared with protein G Dynabeads for 1 h at 4 °C and subsequently incubated at 4 °C overnight with M-280 Streptavidin Dynabeads (Thermo Fisher Scientific). The beads were washed five times in 20 mM Tris pH 8, 250 mM KCl, 1.5 mM $MgCl_2$, 10% glycerol, 2 mM 6-aminocaproic acid (6AA), 10 mM NaF, 1 mM β-

glycerophosphate, 1 mM sodium pyrophosphate and 1× cOmplete Protease Inhibitor Cocktail (Roche) by removal of the supernatant by magnetic sorting. The precipitated proteins were resuspended in 2× SDS sample buffer, eluted from the beads by boiling and separated by SDS-PAGE followed by immunoblotting.

Inverse fluorescence recovery after photobleaching (iFRAP) analysis

In vitro short-term cultured pro-B cells and Pax5-deficient progenitors as well as *ex vivo* sorted splenic mature B cells ($CD43^{-}$) expressing the *Smc3-Gfp* transgene were seeded onto poly-L-lysine-coated glass slides in phenol red-free IMDM in the presence of recombinant IL-7 or BAFF 60-mer ligand (AdipoGen Life Sciences), respectively. Cells were imaged on a LSM710 confocal microscope (Carl Zeiss) at 37 °C in the presence of 5% CO_2, using a 40×/1.4 numerical aperture (N/A) objective. DNA was counterstained with 0.5 μM SiR-Hoechst (SiR-DNA, Spirochrome) for 4 h before the experiment. Two images were acquired before bleaching half of the nucleus by two iterations of a 488 nm laser at maximal intensity, and 240 images were acquired afterwards at 1 min intervals. Signal intensities were measured in bleached and unbleached regions followed by background subtraction using the blue ZEN software (version 2.6). Normalization of the iFRAP curve and curve fitting were performed as described[50].

Mapping of open chromatin regions

Open chromatin regions were mapped in *ex vivo* sorted lymphoid progenitors and different B cell types by the ATAC-seq method as described[51] with the modification that the nuclei were prepared by incubating cells with nuclear preparation buffer (0.3 M sucrose, 10 mM Tris pH 7.5, 60 mM KCl, 15 mM NaCl, 5 mM $MgCl_2$, 0.1 mM EGTA, 0.1% NP-40, 0.15 mM spermine, 0.5 mM spermidine, and 2 mM 6AA) before treatment with the transposase Tn5 (4 μl of Nextera Tn5 transposase per 30,000 cells).

ChIP analysis of transcription factors, epigenetic regulators and histone modifications

Ex vivo sorted and short-term cultured pro-B cells were crosslinked with 1% formaldehyde (Sigma) for 10 min (Pax5, CTCF and histone modification analysis). Nuclei were prepared and lysed in the presence of 0.25% SDS (Pax5, CTCF) or 1% SDS (histone modifications). The chromatin was sheared by sonication with the Bioruptor® Standard (Diagenode), followed by immunoprecipitation with specific antibodies. The specific enrichment was measured and calculated as the precipitated DNA amount relative to input DNA.

For Suz12 and Ezh2 ChIP-seq experiments, short-term cultured control (*Rag2*$^{-/-}$) and Pax5-deficient (*Pax5*$^{-/-}$ *Rag2*$^{-/-}$) pro-B cells as well as activated mature B cells were subjected to crosslinking first with 1% formaldehyde (Sigma) for 10 min followed by 2 mM disuccinimidyl glutarate (DSG, 20593, Thermo Fisher Scientific) for 45 min. Nuclei were prepared and lysed in the presence of 0.25% SDS. Pax5 binding was determined in mature *Pax5*$^{Bio/Bio}$ B cells, which were stimulated with 1.5 mg/ml anti-CD40 (HM40-3, eBioscience) and 10 ng/ml IL-4 for 2 days, followed by Bio-ChIP-seq analysis as described[52]. The ChIP-precipitated DNA (1–2 ng) was used for library preparation and subsequent Illumina deep sequencing (Supplementary Table 5).

VDJ-seq analysis

VDJ-Seq analysis of the *Igh* locus was performed as described[27]. Genomic DNA was extracted from *ex vivo* sorted pro-B cells. The DNA (2 µg) was sheared using the Bioruptor sonicator (Diagenode) and subjected to end-repair and A-tailing, followed by ligation of adapters containing 12 UMI sequences using the NEBNext Ultra II DNA library prep kit from Illumina (NEB). A primer extension step with biotinylated J_H-specific primers generated the single-

stranded DNA products that were captured using Dynabeads MyOne streptavidin T1 beads (Thermo Fisher Scientific) and PCR-amplified with nested J_H-specific and adapter-binding primers (Supplementary Table 4). The llumina sequencing adapter primers including the indexes for multiplexing of libraries were added to the PCR products in a final PCR amplification step. Paired-end 300-bp sequencing was performed on a MiSeq (Illumina) sequencing instrument (Supplementary Table 5).

3C-seq analysis

The 3C-seq method, which is a modified version of the 3C-HTGTS method[23], is based on the VDJ-seq method[27]. In short, 3C-templates were prepared by crosslinking 10^7 short-term cultured pro-B cells in 2% formaldehyde for 10 min, followed by quenching with glycine and cell lysis. Nuclei were subjected to treatment with 0.5% SDS (62 °C, 10 min) and 1.14% Triton X-100 (37 °C, 15 min), and chromatin was digested with DpnII (4x 500 U DpnII (NEB) at 37 °C for 4-5 h), as described[4]. After heat inactivation of DpnII, the chromatin was ligated, then de-crosslinked (0.3 mg/ml proteinase K, 55 °C for 4 hr and 65 °C overnight) and treated with RNase A. Phenol-chloroform extracted DNA (5-6 μg) was used for 3C-seq library preparation by using the VDJ-seq method[27] with viewpoint-specific biotinylated and nested primers (Supplementary Table 4), followed by paired-end 300-bp sequencing on a MiSeq (Illumina) sequencing instrument (Supplementary Table 5).

Complementary DNA (cDNA) preparation for RNA-sequencing

Total RNA from *ex vivo* sorted pro-B and pre-B cells or short-term *in vitro* expanded pro-B cells was isolated with the RNeasy Plus Mini Kit (Qiagen), and mRNA was purified by two rounds of poly(A) selection with the Dynabeads mRNA purification kit (Invitrogen). The mRNA was fragmented by heating at 94 °C for 3 min in fragmentation buffer. The fragmented mRNA was

used as template for first-strand cDNA synthesis with random hexamers and the Superscript Vilo First-Strand Synthesis System (Invitrogen). The second-strand cDNA synthesis was performed with 100 mM dATP, dCTP, dGTP and dUTP in the presence of RNase H, *E. coli* DNA polymerase I and DNA ligase (Invitrogen).

Library preparation and Illumina deep sequencing

About 0.6-20 ng of cDNA or ChIP-precipitated DNA was used as starting material for the generation of sequencing libraries with the NEBNext Ultra II DNA library prep kit for Illumina (NEB). Alternatively, sequencing libraries were generated using the NEBNext End Repair/dA-Tailing Module and NEBNext Ultra Ligation Module (NEB) followed by amplification with the KAPA Real-Time Amplification kit (KAPA Biosystems). Cluster generation and sequencing were carried out using the Illumina HiSeq 2500 system with a read length of 50 nucleotides, according to the manufacturer's guidelines.

Hi-C library preparation

$CD19^+$ pro-B cells or $B220^+$ Pax5-deficient progenitors, which were isolated from the bone marrow by immunomagnetic enrichment with anti-CD19- or B220-MicroBeads (Milteny Biotec), respectively, were cultured for 4-12 days on OP9 cells in IL-7-containing IMDM[48]. Prior to Hi-C library preparation, the cultured $CD19^+$ pro-B cells or $B220^+$ Pax5-deficient progenitors were purified by immunomagnetic enrichment with anti-CD19- or B220-MicroBeads (Milteny Biotec) to eliminate contaminating OP9 feeder cells. The $CD19^+$ pro-B cells were additionally depleted of IgM-expressing cells. Mature $CD43^-$ B cells were isolated from the spleen with the B Cell Isolation Kit (mouse; Milteny Biotec), which depleted CD43-expressing immature B cells and non-B cells following staining with biotin-conjugated anti-CD43, anti-CD4

and anti-Ter119 antibodies and subsequent depletion with Anti-Biotin Microbeads. Hi-C libraries were prepared from 2×10^7 cells as described in detail[4] and were sequenced using the Illumina NextSeq system with a read length of 75 nucleotides in the paired-end mode, according to the manufacturer's guidelines.

Identification of CTCF peaks in the *Igh* locus

We identified CTCF peaks (here referred to as CTCF-binding elements; CBEs) in the *Igh* locus based on the published data of our CTCF antibody ChIP-seq experiment (GSM114565) that was performed with short-term cultured *Rag2*$^{-/-}$ pro-B cells[18]. Sequence reads were uniquely aligned to the mouse genome assembly version of July 2007 (NCBI37/mm9) using the Bowtie program version 1.0 (ref. 53). CTCF peaks were called by MACS 1.3.6.1 (ref. 54) and filtered for *P* values of $< 10^{-10}$ to obtain a total of 97,487 peaks. We subsequently split all 166 peaks called in the *Igh* locus (mm9, Chr.12; 114,451,520-117,269,160) using PeakSplitter[55] with height cutoff parameter 10 and valley parameter 0.4, and applied a conservative height cutoff of 100 reads to obtain a final list of peaks. This resulted in 137 CBEs: 10 CBEs at the 3' end, 2 CBEs in the IGCR1 region and 125 CBEs within the V_H gene cluster (Extended Data Fig 1a). The inverted region (mm9 Chr12: 116,237,220-117,126,667) of the *Igh*$^{890\text{-inv}}$ allele contained 49 CBEs.

To enumerate all potential CTCF-binding sites in the *Igh* locus, we retrieved the repeat-masked mouse genome sequence (mm9) using EXONERATE[56] and scanned the sequence region of the *Igh* locus with a CTCF motif derived from the summits of the top 300 CTCF peaks, using MEME[57]. The scanning was done with FIMO version 4.9.1 (ref. 57) by setting the *P* value threshold to < 0.001, which resulted in 994 (forward) and 791 (reverse) hits (Extended Data Fig 1a). For 115 of the 137 CBEs, we could assign a clear CTCF motif within 25 bp from the peak

summit. Within the inverted region of the *Igh*$^{890\text{-inv}}$ allele, 37 of the 49 CBEs contained a CTCF motif.

Definition of the 5' and 3' ends of the mouse *Igh* locus

For this paper, we defined the extent of the *Igh* locus according to its loop domain (TAD) in pro-B cells starting with the first interacting CTCF peak (second peak upstream of V_H1-86 gene) to the last of the 10 CTCF peaks in the 3'CBE region. We furthermore added 2 kb from the summit of these two CTCF peaks, which resulted in the following Chr. 12 mm9 coordinates for the mouse C57BL/6 *Igh* locus; 114,451,520 (3' end) - 117,269,160 (5' end) with a length of 2,817,641 bp.

Design of the CTCF-binding site array

We selected the top 20 CTCF peaks from the *Igh* locus (Extended Data Fig. 3a), extracted a 24-bp sequence containing the forward CTCF-binding motif, added the flanking 10 bp after random sequence shuffling[57] and added another 20 bp of random sequence, which result in an 84-bp sequence (Supplementary Table 1c). Care was taken not to create an additional CTCF or Pax5 motif in the shuffling process. The 20 CTCF-binding sequences were concatenated to generate an array of 20 CBEs, which was inserted in forward or reverse orientation at position 116,242,836 of the *Igh* locus (Extended Data Fig 3a).

Analysis of RNA-seq data

The number of reads per gene was counted using the featureCounts version 1.5.0 (ref. 58) with default settings. Transcripts per million (TPM) values were calculated as described[59]. Differential gene expression between *ex vivo* sorted *Wapl*$^{+/+}$ and *Wapl*$^{\Delta P1,2/\Delta P1,2}$ pro-B cells was analysed using R version 3.3.3. and DESeq2 version 2.1.14.1. Regularized log

transformations were computed with the blind option set to 'FALSE'. Genes with an adjusted *P* value < 0.05, TPM (averaged for each genotype) > 5 at least in one of the two genotypes, and a fold-change of > 2 were called as significantly differentially expressed (Extended Data Fig. 10e and Supplementary Table 3). All transcripts of the V, D and J gene segments at the *Igh*, *Igk* and *Igl* loci were eliminated from the list of significantly regulated genes, although the immunoglobulin and T cell receptor transcripts were included in all TPM calculations.

Differential gene expression between *ex vivo* sorted control and *Rag1*$^{Cre/+}$ *Eed*$^{fl/fl}$ pro-B cells was analysed as described above, except that only genes with an expression difference of > 3-fold were considered (Extended Data Fig. 9f and Supplementary Table 2). The control samples consisted of 3 independent experiments performed with *Rag1*$^{Cre/+}$ *Eed*$^{fl/+}$ pro-B cells and 1 experiment performed with *Eed*$^{fl/fl}$ pro-B cells (Supplementary Table 5).

Bioinformatic analysis of 3C-seq data

We analysed the 3C-seq data with the captureC 2.0 program[60] with newer versions of the programs cutadapt 1.16 (ref. 61) and trim_galore 0.4.2 (https://www.bioinformatics.babraham.ac.uk/projects/trim_galore/). For comparison, the 3C-seq reads were mapped as normalized counts by normalizing to the number of viewpoint-containing reads of the smallest library in the set of samples compared. The 3C-seq data were further analysed with r3Cseq 1.28 (ref. 62) with minor modifications to adjust for a larger viewing range required for the *Igh* locus and for the insertion of the CBE array by generating modified genome versions. The mean RPM values shown in Fig. 1c and Extended Data Fig. 4b,d have been calculated by r3Cseq, using a customized script based on the R version 3.3.3. For the generation of the 3C-seq data shown in Extended Data Figs. 2c and 4e,f, we used the r3Cseq command 'getBatchInteractions' with the option 'union' for analyzing the 3C-seq data of the two replica

experiments performed with pro-B cells of each genotype. The *Igh* regions analysed in Fig. 1b,c were defined by the following mm9 coordinates on chromosome 12: A (117,126,669-117,270,000), B (116,237,129-117,126,668), C (115,000,000-116,237,128) and D (114,451,520-114,999,999). The *Igh* regions analysed in Extended Data Fig. 4a-d were defined as follows: A (116,292,840-116,592,840) and B (115,892,840-116,192,840).

Bioinformatic analysis of VDJ-seq data

The bioinformatic analysis of the VDJ-seq data was performed as described in detail[27], and the resulting data was summarised using customised scripts based on the R version 3.3.3.

Processing, normalization and resolution of Hi-C data

The HiCUP pipeline version 0.5.10 (ref. 63) with the scorediff parameter set to "10" was used to truncate, align and filter the reads by applying the following software versions: R 3.4.1 9 (https://www.r-project.org), Bowtie 2.2.9 (ref. 53) and SAMtools 1.4. (ref. 64). We merged the data of the two Hi-C experiments, which were performed with progenitor or pro-B cells of the same genotype, to produce contact matrix files with the Juicer tools 1.8.9 (ref. 30). The resolution of the Hi-C data has been calculated according to Rao et al.[4] by using the script “calculate_map_resolution”. The following unique di-tags were generated; 382,665,804 (*Pax5*$^{\Delta/\Delta}$ progenitors), 314,876,625 (*Wapl*$^{+/+}$ pro-B cells), 306,800,111 (*Wapl*$^{\Delta P1,2/\Delta P1,2}$ pro-B cells) and 111,531,239 (*Wapl*$^{+/+}$ mature B cells). The following resolution of the Hi-C data (Fig. 5b-f) was calculated; 5.4 kb (*Pax5*$^{\Delta/\Delta}$ progenitors), 6.7 kb (*Wapl*$^{+/+}$ pro-B cells), 7.25 kb (*Wapl*$^{\Delta P1,2/\Delta P1,2}$ pro-B cells) and 28.6 kb (*Wapl*$^{+/+}$ mature B cells).

Analysis of intra-chromosomal contact frequency (Hi-C)

Contact frequency distributions have been calculated using the makeTagDirectory command of HOMER 4.10.3 (ref. 65). The contact frequency plots shown in Fig. 5b and Extended Data Fig. 10b are based on ~50 contact data points based on ~50 bins, whereby each bin is defined as 0.1 step on the $\log_{10}$ scale of genomic distance observed between the contract points. Each data point is thus the sum of all contact fraction values in the respective bin. The contact frequency plot is shown as a smoothened line of the ~50 contact data points plotted against the logarithmic ($\log_{10}$) genomic distance.

Analysis of chromatin loops and compartments (Hi-C)

Intra-chromosomal loops have been called with the HiCCUPS algorithm from the Juicer tools[30]. The distribution of the loop length has been calculated by custom R and bash scripts. The compartments shown in Fig. 5c were calculated and visualized with Juicebox[4].

Statistical analysis

Statistical analysis was performed with the GraphPad Prism 7 software. Two-tailed unpaired Student's *t*-test analysis was used to assess the statistical significance of one observed parameter between two experimental groups. If more than one parameter were measured in two experimental groups, multiple *t*-tests were applied, and the Holm-Sidak multi comparison test was used to report the significance between the two groups. One-way ANOVA was used when more than two experimental groups were compared, and the statistical significance was determined by the Tukey post hoc test. The statistical evaluation of the RNA-seq data was performed with the DESeq2 program.

Reporting summary

Further information on the research design is available in the Nature Research Reporting Summary linked to this paper.

Data availability

The RNA-seq, ChIP-seq, ATAC-seq, VDJ-seq, 3C-seq and Hi-C data reported in this study (Supplementary Table 5) are available at the Gene Expression Omnibus (GEO) repository under the accession number GSE140975. Figure source data are provided for this paper.

References

31. Urbánek, P., Wang, Z.-Q., Fetka, I., Wagner, E. F. & Busslinger, M. Complete block of early B cell differentiation and altered patterning of the posterior midbrain in mice lacking Pax5/BSAP. *Cell* **79**, 901-912 (1994).
32. Horcher, M., Souabni, A. & Busslinger, M. Pax5/BSAP maintains the identity of B cells in late B lymphopoiesis. *Immunity* **14**, 779-790 (2001).
33. McManus, S. *et al.* The transcription factor Pax5 regulates its target genes by recruiting chromatin-modifying proteins in committed B cells. *EMBO J.* **30**, 2388-2404 (2011).
34. Fuxa, M. & Busslinger, M. Reporter gene insertions reveal a strictly B lymphoid-specific expression pattern of *Pax5* in support of its B cell identity function. *J. Immunol.* **178**, 3031-3037 (2007).
35. Shinkai, Y. *et al.* RAG-2-deficient mice lack mature lymphocytes owing to inability to initiate V(D)J rearrangement. *Cell* **68**, 855-867 (1992).
36. Krimpenfort, P. *et al.* p15Ink4b is a critical tumour suppressor in the absence of p16Ink4a. *Nature* **448**, 943-946 (2007).
37. Tallquist, M. D. & Soriano, P. Epiblast-restricted Cre expression in MORE mice: a tool to distinguish embryonic vs. extra-embryonic gene function. *Genesis* **26**, 113-115 (2000).
38. McCormack, M. P., Forster, A., Drynan, L., Pannell, R. & Rabbitts, T. H. The LMO2 T-cell oncogene is activated via chromosomal translocations or retroviral insertion during gene therapy but has no mandatory role in normal T-cell development. *Mol. Cell. Biol.* **23**, 9003-9013 (2003).

39. Hobeika, E. *et al.* Testing gene function early in the B cell lineage in mb1-cre mice. *Proc. Natl. Acad. Sci. USA* **103**, 13789-13794 (2006).
40. Seibler, J. *et al.* Rapid generation of inducible mouse mutants. *Nucleic Acids Res.* **31**, e12 (2003).
41. de Boer, J. *et al.* Transgenic mice with hematopoietic and lymphoid specific expression of Cre. *Eur. J. Immunol.* **33**, 314-325 (2003).
42. Rodriguez, C. I. *et al.* High-efficiency deleter mice show that FLPe is an alternative to Cre-*loxP*. *Nat. Genet.* **25**, 139-140 (2000).
43. Anastassiadis, K. *et al.* Dre recombinase, like Cre, is a highly efficient site-specific recombinase in *E. coli*, mammalian cells and mice. *Dis. Model. Mech.* **2**, 508-515 (2009).
44. Singla, V. *et al.* Floxin, a resource for genetically engineering mouse ESCs. *Nat. Methods* **7**, 50-52 (2010).
45. Yang, H. *et al.* One-step generation of mice carrying reporter and conditional alleles by CRISPR/Cas-mediated genome engineering. *Cell* **154**, 1370-1379 (2013).
46. Poser, I. *et al.* BAC TransgeneOmics: a high-throughput method for exploration of protein function in mammals. *Nat. Methods* **5**, 409-415 (2008).
47. Adams, B. *et al. Pax-5* encodes the transcription factor BSAP and is expressed in B lymphocytes, the developing CNS, and adult testis. *Genes Dev.* **6**, 1589-1607 (1992).
48. Nutt, S. L., Urbánek, P., Rolink, A. & Busslinger, M. Essential functions of Pax5 (BSAP) in pro-B cell development: difference between fetal and adult B lymphopoiesis and reduced *V*-to-*DJ* recombination at the *IgH* locus. *Genes Dev.* **11**, 476-491 (1997).
49. Minnich, M. *et al.* Multifunctional role of the transcription factor Blimp-1 in coordinating plasma cell differentiation. *Nat. Immunol.* **17**, 331-343 (2016).
50. Holzmann, J. *et al.* Absolute quantification of cohesin, CTCF and their regulators in human cells. *eLife* **8**, e46269 (2019).
51. Buenrostro, J. D., Giresi, P. G., Zaba, L. C., Chang, H. Y. & Greenleaf, W. J. Transposition of native chromatin for fast and sensitive epigenomic profiling of open chromatin, DNA-binding proteins and nucleosome position. *Nat. Methods* **10**, 1213-1218 (2013).
52. Revilla-i-Domingo, R. *et al.* The B-cell identity factor Pax5 regulates distinct transcriptional programmes in early and late B lymphopoiesis. *EMBO J.* **31**, 3130-3146 (2012).
53. Langmead, B. Aligning short sequencing reads with Bowtie. *Curr. Protoc. Bioinformatics* Chapter 11, Unit 11.7 (2010).
54. Zhang, Y. *et al.* Model-based analysis of ChIP-Seq (MACS). *Genome Biol.* **9**, R137 (2008).

55. Salmon-Divon, M., Dvinge, H., Tammoja, K. & Bertone, P. PeakAnalyzer: genome-wide annotation of chromatin binding and modification loci. *BMC Bioinformatics* **11**, 415 (2010).
56. Slater, G. S. & Birney, E. Automated generation of heuristics for biological sequence comparison. *BMC Bioinformatics* **6**, 31 (2005).
57. Machanick, P. & Bailey, T. L. MEME-ChIP: motif analysis of large DNA datasets. *Bioinformatics* **27**, 1696-1697 (2011).
58. Liao, Y., Smyth, G. K. & Shi, W. featureCounts: an efficient general purpose program for assigning sequence reads to genomic features. *Bioinformatics* **30**, 923-930 (2014).
59. Wagner, G. P., Kin, K. & Lynch, V. J. Measurement of mRNA abundance using RNA-seq data: RPKM measure is inconsistent among samples. *Theory Biosci.* **131**, 281-285 (2012).
60. Davies, J. O. *et al.* Multiplexed analysis of chromosome conformation at vastly improved sensitivity. *Nat. Methods* **13**, 74-80 (2016).
61. Martin, M. Cutadapt removes adapter sequences from high-throughput sequencing reads. *EMBnet J.* **17**, 10-12 (2011).
62. Thongjuea, S., Stadhouders, R., Grosveld, F. G., Soler, E. & Lenhard, B. r3Cseq: an R/Bioconductor package for the discovery of long-range genomic interactions from chromosome conformation capture and next-generation sequencing data. *Nucleic Acids Res.* **41**, e132 (2013).
63. Wingett, S. *et al.* HiCUP: pipeline for mapping and processing Hi-C data. *F1000Res.* **4**, 1310 (2015).
64. Li, H. *et al.* The Sequence Alignment/Map format and SAMtools. *Bioinformatics* **25**, 2078-2079 (2009).
65. Heinz, S. *et al.* Simple combinations of lineage-determining transcription factors prime *cis*-regulatory elements required for macrophage and B cell identities. *Mol. Cell* **38**, 576-589 (2010).

Acknowledgements

We thank William C. Skarnes for advice and help with the Floxin method, M. Leeb for assistance with ES cell derivation, E. Lieberman Aiden for discussion, R. Stocsits for advice with Hi-C analysis, K. Aumayr's team for flow cytometric sorting, C. Theussl's team for generating gene-modified mice and A. Sommer's team at the Vienna BioCenter Core Facilities

for Illumina sequencing. This research was supported by Boehringer Ingelheim, the European Research Council (ERC) under the European Union's Horizon 2020 research and innovation program (grant agreement No 740349-PlasmaCellControl and No 693949-CohesinMolMech), the Austrian Industrial Research Promotion Agency (Headquarter Grant FFG-852936), the Human Frontier Science Program grant RGP0057/2018 (to J.-M.P.) and a long-term fellowship from the Human Frontier Science Program LT001527/2017 (to K.N.).

Author contributions

L.H. did most experiments; A.E. generated and analysed the *Eed* mutant mouse; G.W. generated the Hi-C data; K.N. performed the iFRAP analyses; H.T. performed ATAC-seq analyses and contributed to 3C-seq experiments; D.K.-P. performed RT-qPCR analyses; K.S. generated the *Igh*$^{CBE/+}$ and *Igh*$^{CBE\text{-}inv/+}$ mice and inserted the V_H8-8 gene into *Igh*$^{\Delta 890/+}$ ES cells; Q.S. generated the transgenic *Smc3-Gfp* mouse and contributed to the generation of the *Igh*$^{fl\text{-}890\text{-}fl/+}$ mouse; P.B. performed the PRC2-Pax5 recruitment experiments; M.J. performed most bioinformatic analyses (RNA-seq, VDJ-seq, 3C-seq and Hi-C data); M.F. analysed the *Eed* RNA-seq data; J.-M.P. provided advice on cohesin biology and the design of iFRAP and Hi-C experiments; L.H. and M.B. planned the project, designed the experiments and wrote the manuscript.

Competing interests

The authors declare no competing financial interests.

Extended Data Figures Legends

Extended Data Fig. 1 | Generation and characterization of the *Igh*$^{890\text{-inv}}$ allele.

a, Orientation of the CTCF-binding sites in the *Igh* locus. The CTCF-binding pattern was determined by ChIP-seq of *Rag2*$^{-/-}$ pro-B cells. The locations of forward (red) and reverse (blue) CTCF motifs detected at the summit of the CTCF peaks are shown together with all predicted CTCF motifs, identified based on the forward and reverse consensus CTCF-binding motifs shown. The annotation of the C57BL/6 *Igh* locus indicates the distinct V_H gene families (different colours) in the distal, middle and proximal V_H gene regions (Johnston *et al.* 2006. *J. Immunol*. 176, 4221-4234) and the 3' proximal *Igh* domain containing the D_H, J_H and C_H elements as well as the Eμ and 3'RR enhancers (red). **b**, Schematic diagram of the *Igh*$^{\text{ifl-890-fl}}$ and *Igh*$^{890\text{-inv}}$ alleles. The indicated selection cassettes were used for introducing the upstream inverted *lox*71 site (ifl) and downstream *lox*P site (fl) by sequential ES cell targeting. **c**, Flow cytometric analysis of bone marrow cells from *Igh*$^{890\text{-inv}/890\text{-inv}}$ and *Igh*$^{+/+}$ mice. The relative frequencies of the indicated cell types (defined in Methods) are shown as mean values with SEM. **d**, Flow cytometric determination of the ratio of immature IgM^b (B6) to IgM^a (129) B cells from *Igh*$^{890\text{-inv(B6)}/+(129)}$ and *Igh*$^{+(B6)/+(129)}$ mice, which were generated by crossing *Igh*$^{890\text{-inv}/+}$ mice on the C57BL/6 (B6) background with *Igh*$^{+/+}$ mice of the 129/Sv (129) strain. The rearranged *Igh* alleles of the C57BL/6 and 129/Sv strains give rise to expression of the IgM^b and IgM^a isotypes, respectively. **e**, V_H gene expression from the *Igh*$^{890\text{-inv(B6)}}$ or *Igh*$^{+(B6)}$ allele in immature IgM^b (B6) B cells sorted from *Igh*$^{890\text{-inv(B6)}/+(129)}$ or *Igh*$^{+(B6)/+(129)}$ mice, respectively. The RNA-seq profiles are shown with the *Igh* annotation (see **a**) and inverted

region (bar). One of two experiments is shown. RPM, reads per million mapped sequence reads. **f**,**g** VDJ-seq analysis of pro-B cells from the bone marrow of *Igh*$^{890\text{-inv}/890\text{-inv}}$ and *Igh*$^{+/+}$ mice. **f**, The percentages of uniquely identified DJ_H and VDJ_H sequences are indicated. **g**, The relative usage of the distal V_H genes at the *Igh* 5' end is shown as mean percentage of all VDJ_H recombination events with SEM. A horizontal bar indicates the 5' end of the inverted region. Statistical data are shown as mean value with SEM and were analysed either by multiple *t*-tests (unpaired and two-tailed with Holm-Sidak correction; **c**,**f**) or by the Student's *t*-test (unpaired and two-tailed; **d**). *n*, number of mice (**c**,**d**) or experiments (**f**,**g**). Each dot corresponds to one mouse.

Extended Data Fig. 2 | Dependence of V_H-DJ_H recombination on chromatin looping and V_H gene orientation. a, ChIP-seq analysis of CTCF binding in the distal 890-kb region in short-term cultured pro-B cells from *Igh*$^{890\text{-inv}/890\text{-inv}}$ and *Igh*$^{+/+}$ mice. Vertical bars indicated CTCF peaks defined by 'peak calling'. The ChIP-seq data of the *Igh*$^{890\text{-inv}}$ allele were aligned on the wild-type *Igh* sequences. One of two experiments per genotype is shown. **b**, *Igh* positions of the 3C-seq viewpoints, which are referred to by the nearest V_H gene, the hypersensitive site 5 (HS5) in the 3'CBE region or the CBE array insertion (Supplementary Table 1c). **c**, Interactions from the 5' (V_H1-86; left) and 3' (HS5; right) viewpoints in short-term cultured pro-B cells from *Igh*$^{890\text{-inv}/890\text{-inv}}$ *Rag2*$^{-/-}$ and *Igh*$^{+/+}$ *Rag2*$^{-/-}$ mice. The 3C-seq reads along the *Igh* locus (upper two panels) are shown as RPM values with the respective *Q* values, which were calculated by the r3Cseq program based on two 3C-seq experiments per genotype. The lower panel shows the fold-change of the RPM values for interaction differences of > 2-fold (dashed line) between experimental (Exp) *Igh*$^{890\text{-inv}/890\text{-inv}}$ *Rag2*$^{-/-}$ and control (Ctrl) *Igh*$^{+/+}$ *Rag2*$^{-/-}$ pro-B cells. **d,**

Schematic diagram summarising the loop formation at the *Igh*$^{890\text{-inv}}$ allele in pro-B cells. The CBEs with their orientation are indicated by red and blue arrowheads, V_H genes by grey arrows and loops by arches. The new loop domain is indicated in red. **e**, Schematic diagram of the *Igh*$^{\Delta 890}$, *Igh*$^{V8\text{-}8}$ and *Igh*$^{V8\text{-}8\text{-}inv}$ alleles. The *Igh*$^{V8\text{-}8}$ and *Igh*$^{V8\text{-}8\text{-}inv}$ alleles were generated by insertion of the V_H8-8 gene with 500 bp of its 5' and 3' flanking sequences (lacking any CBE) in the forward or reverse orientation at the deletion point (117,126,667 / 116,237,220; mm9, Chr. 12) of the *Igh*$^{\Delta 890}$ allele (see Methods). The distances from the 3' end of the V_H8-8 gene to the next CBEs and V_H genes are indicated. The sequence of the inserted V_H8-8 with its flanking DNA sequences is shown in Supplementary Table 1b. **f**, RNA-seq profile of the *Igh* locus in immature B cells from the bone marrow of *Igh*$^{V8\text{-}8/\Delta 890}$, *Igh*$^{V8\text{-}8\text{-}inv/\Delta 890}$ and *Igh*$^{+/\Delta 890}$ mice. The V_H8-8 gene position and *Igh* annotation are indicated. The data of one of two RNA-seq experiments per genotype is shown. **g**, V_H8-8 mRNA expression in immature B-cells of the indicated genotypes is shown as mean TPM (transcripts per million) value. Each dot corresponds to one experiment.

Extended Data Fig. 3 | Characterization of *Igh* alleles with inserted CBE arrays.

a, Insertion of an array of 20 functional CBEs in forward (red) or inverted (inv, blue) orientation at position 116,242,836 (mm9, Chr. 12) in the *Igh*^{CBE} or *Igh*$^{CBE\text{-}inv}$ allele, respectively. The positions of the *Igh* CBEs used for the generation of the CBE arrays (Supplementary Table 1c) are indicated below a map of all CBEs. **b**, CTCF binding at the *Igh* locus, as determined by ChIP-seq analysis of short-term cultured pro-B cells from the bone marrow of *Igh*$^{CBE\text{-}inv/CBE\text{-}inv}$ and *Igh*$^{CBE/CBE}$ mice. One of two experiments is shown. **c**, Flow cytometric determination of the ratio of immature IgM^b (B6) to IgM^a (129) B cells in the bone marrow of *Igh*$^{CBE\text{-}}$

$^{inv(B6)/+(129)}$, *Igh*$^{CBE(B6)/+(129)}$ and *Igh*$^{+(B6)/+(129)}$ mice (see Extended Data Fig. 1d). The IgM^{b} / IgM^{a} ratios are shown relative to that of immature B cells of *Igh*$^{+(B6)/+(129)}$ mice (set to 1). Statistical data are shown as mean value with SEM and were analysed by one-way ANOVA with Tukey's post-hoc test. **d**, V_H gene expression from the *Igh*$^{CBE\text{-}inv(B6)}$, *Igh*$^{CBE(B6)}$ and *Igh*$^{+(B6)}$ alleles in immature IgM^{b} (B6) B cells sorted from *Igh*$^{CBE\text{-}inv(B6)/+(129)}$, *Igh*$^{CBE(B6)/+(129)}$ and *Igh*$^{+(B6)/+(129)}$ mice, respectively (see Extended Data Fig. 1d). The expression (TPM) value of each V_H gene is shown as shared (grey) and unique expression of the *Igh*$^{CBE\text{-}inv(B6)}$ (blue), *Igh*$^{CBE(B6)}$ (green) and *Igh*$^{+(B6)}$ (black) alleles. Mean TPM values with SEM were determined by the DESeq2 program and are based on two (*Igh*$^{CBE\text{-}inv(B6)}$, *Igh*$^{CBE(B6)}$) and three (*Igh*$^{+(B6)}$) RNA-seq experiments. The V_H genes are aligned according to their *Igh* position. **e**,**f**, VDJ-seq analysis of *ex vivo* sorted pro-B cells from the bone marrow of *Igh*$^{+/+}$, *Igh*$^{CBE/CBE}$ and *Igh*$^{CBE\text{-}inv/CBE\text{-}inv}$ mice. **e**, The percentages of uniquely identified DJ_H and VDJ_H sequences are shown as mean percentage with SEM. **f**, Pairwise comparisons of VDJ-seq results obtained with *Igh*$^{+/+}$ (black), *Igh*$^{CBE/CBE}$ (green) and *Igh*$^{CBE\text{-}inv/CBE\text{-}inv}$ (blue) pro-B cells. The relative usage of each V_H gene was determined as percentage of all VDJ_H recombination events and is shown as mean percentage with SEM. *n*, number of mice. Each dot corresponds to one mouse (**c**,**e**).

Extended Data Fig. 4 | New loop formation upon insertion of an inverted CBE array in the *Igh* locus. a-d, 3C-seq analysis of interactions across the *Igh* locus from the 3' (HS5; **a**,**b**) or 5' (CBE; **c**,**d**) viewpoint in short-term cultured *Igh*$^{CBE\text{-}inv/CBE\text{-}inv}$, *Igh*$^{CBE/CBE}$ and *Igh*$^{+/+}$ pro-B cells. **a**,**c**, Mapping of the 3C-seq reads as normalized counts across the *Igh* locus. One of two

experiments per genotype is shown. **b**,**d**, Quantification of the interactions from the 3' (HS5, **b**) or 5'(CBE, **d**) viewpoint. The 3C-seq reads in regions A and B were quantified as mean RPM value per region, based on two experiments per genotype. **e**,**f**, Interactions from the 3' (HS5; **e**) or 5' (CBE; **f**) viewpoint in *Igh*$^{+/+}$, *Igh*$^{CBE/CBE}$ and *Igh*$^{CBE\text{-}inv/CBE\text{-}inv}$ pro-B cells. The 3C-seq reads along the *Igh* locus (upper two panels) are shown as RPM values with the respective *Q* values, calculated by the r3Cseq program based on two experiments per genotype. Arrows highlight a strong interaction from the 3' viewpoint (HS5) to a region immediately downstream of the inserted CBE array (**e**), and a bar denotes the 600-kb region exhibiting reduced interactions in *Igh*$^{CBE\text{-}inv/CBE\text{-}inv}$ pro-B cells (**e**). The lower panel shows the fold-change of the RPM values for interaction differences of > 2-fold (dashed line; **e**) or > 1.5-fold (**f**) between the experimental (Exp) and control (Ctrl) pro-B cells of the indicated genotypes. **g**, Schematic diagram summarising the loop formation at the *Igh*$^{CBE\text{-}inv}$ allele in pro-B cells. The CBEs with their orientation are indicated by red and blue arrowheads, V_H genes by grey arrows and loops by arches. The new loop domain is indicated in red. A thicker blue arche indicates the enhanced interaction from the 3'CBE to a region immediately downstream of the inserted CBE array.

Extended Data Fig. 5 | Cohesin stabilization on chromatin by Pax5-dependent *Wapl* repression in pro-B cells. a, *Wapl* mRNA expression in developing and mature B and T cells of wild-type mice. The indicated B and T cell types were sorted from the bone marrow (pro-B, pre-B cells), thymus (DN, DP, CD4$^+$, CD8$^+$ T cells) or spleen (mature B, CD4$^+$ and CD8$^+$ T cells). The *Wapl* mRNA expression of the different cell types was determined by RT-qPCR analysis relative to *Tbp* expression and is shown relative to that of pro-B cells (set to 1). The expression data are shown as mean values with SEM, based on four RT-qPCR experiments per cell type. **b**, Wapl protein expression in *ex vivo* sorted *Rag2*$^{-/-}$ pro-B cells from the bone marrow and wild-

type mature B cells from the spleen and lymph nodes, as determined by immunoblotting of 3-fold serially diluted whole-cell extracts with antibodies detecting Wapl or TBP. One of two experiments is shown with marker proteins (kilodaltons). **c**, B cell development in the bone marrow of *Smc3-Gfp* transgenic (green) and wild-type (black) mice, as determined by flow cytometry. The relative frequencies of the indicated cell types are shown as mean values with SEM (left). GFP expression in selected cell types is shown (right). **d**, Interaction of the Smc3-GFP protein with other cohesin subunits in short-term cultured *Smc3-Gfp* pro-B cells. Endogenous Smc1, Scc1 (Rad21), Wapl, Pds5a and Pds5b proteins were co-precipitated with Smc3-GFP from whole-cell extracts of *Smc3-Gfp* or wild-type pro-B cells with an anti-GFP antibody. The input (1/10) and protein precipitate were analysed by immunoblotting with antibodies detecting the indicated cohesin proteins. Smc3ac, acetylated Smc3. One experiment was performed. **e**, Images of one of 16 or 24 iFRAP experiments performed with *Smc3-Gfp* pro-B or mature B cells, respectively. The fluorescence intensities of SiR-Hoechst (pink) and GFP (green) are false-coloured. Scale bar, 10 μm. **f**, Identification of open chromatin regions at the *Wapl* locus by ATAC-seq of the indicated progenitor and B cell types. MPPs, ALPs, pro-B and mature B cells were sorted from wild-type bone marrow or lymph nodes (mature B). Activated B cells and plasmablasts were generated by *in vitro* LPS stimulation of mature B cells. hCD2^{-} (Pax5^{-}) and hCD2^{+} (Pax5^{+}) BLPs were sorted from bone marrow of *Pax5*$^{ihCd2/ihCd2}$ mice, and *Pax5*$^{\Delta/\Delta}$ progenitors from *Vav*-Cre *Pax5*$^{fl/fl}$ *Rag2*$^{-/-}$ mice. *n*, number of mice. Each dot corresponds to one mouse (**a**,**c**). The different cell types are defined in Methods.

Extended Data Fig. 6 | Generation and analysis of *Wapl* mutant mice. a, Mutations introduced at the Pax5-binding sites P1 and P2 in the *Wapl*$^{\Delta P1,2}$, *Wapl*$^{\Delta P1}$ and *Wapl*$^{\Delta P2}$ alleles by CRISPR/Cas9-mediated mutagenesis. The consensus Pax5 motif and the extent of the

deletions (red) are indicated. **b**, Loss of Pax5 binding at the mutated P1 site in *Wapl*$^{\Delta P1/\Delta P1}$ pro-B cells. One of two ChIP-seq experiments is shown. **c**. *Wapl* mRNA expression in short-term cultured *Wapl*$^{\Delta P1,2/\Delta P1,2}$ and *Wapl*$^{+/+}$ pro-B cells is shown as mean TPM value with SEM. *n*, number of RNA-seq experiments. **d**, Wapl protein expression in short-term cultured *Wapl*$^{\Delta P1,2/\Delta P1,2}$ *Rag2*$^{-/-}$ and *Wapl*$^{+/+}$ *Rag2*$^{-/-}$ pro-B cells was determined by immunoblotting of 2-fold serially diluted whole-cell extracts with antibodies detecting Wapl or TBP. One of two experiments is shown with marker proteins (kilodaltons). **e**, *Wapl* mRNA expression in *ex vivo* sorted *Wapl*$^{\Delta P1,2/\Delta P1,2}$ (blue), *Wapl*$^{\Delta P1,2/+}$ (light blue) and *Wapl*$^{+/+}$ (black) pro-B and pre-B cells, *Pax5*$^{\Delta/\Delta}$ progenitors (green; *Vav*-Cre *Pax5*$^{fl/fl}$) as well as *Wapl*$^{\Delta P1,2/\Delta P1,2}$ and *Wapl*$^{+/+}$ T cell subsets from the thymus and spleen, as determined by RT-qPCR analysis relative to *Tbp* expression. The *Wapl* expression of each cell type is indicated relative to that of the *Wapl*$^{+/+}$ cells (set to 1) and is shown as mean value with SEM, based on 2-4 independent RT-qPCR experiments for each cell type and genotype. Each dot (**c**,**e**) corresponds to one mouse. The different cell types are defined in Methods.

Extended Data Fig. 7 | B cell development in *Wapl* mutant mice. a,**b**, *Wapl* expression in *ex vivo* sorted *Wapl*$^{\Delta P1/\Delta P1}$ (blue), *Wapl*$^{\Delta P1/+}$ (light blue) and *Wapl*$^{+/+}$ (black) pro-B and pre-B cells (**a**) as well as in *Wapl*$^{\Delta P2/\Delta P2}$ (blue) and *Wapl*$^{+/+}$ (black) pro-B cells (**b**), as determined by RT-qPCR analysis relative to *Tbp* expression. The *Wapl* expression of each cell type is shown as mean value with SEM relative to that of *Wapl*$^{+/+}$ cells (set to 1). Each dot corresponds to one RT-qPCR experiment performed with sorted cells from one mouse. **c**,**d**, Flow cytometric analysis of bone marrow from *Wapl*$^{\Delta P2/\Delta P2}$ (blue), *Wapl*$^{\Delta P2/+}$ (light blue) and *Wapl*$^{+/+}$ (black)

mice (**c**). The frequencies of the indicated cell types are shown as mean values with SEM (**d**). **e**, Flow cytometric analysis of bone marrow from *Cd79a*$^{Cre/+}$ *Wapl*$^{fl/fl}$ and *Cd79a*$^{Cre/+}$ *Wapl*$^{+/+}$ mice. **f**,**g**, Frequencies of total B, pro-B and pre-B cells are shown for *Cd79a*$^{Cre/+}$ *Wapl*$^{fl/fl}$, *Cd79a*$^{Cre/+}$ *Wapl*$^{fl/+}$ and control mice (**f**) as well as for *Rag1*$^{Cre/+}$ *Wapl*$^{fl/fl}$, *Rag1*$^{Cre/+}$ *Wapl*$^{fl/+}$ and control mice (**g**). The control mice in (**f**) were 3× *Cd79a*$^{Cre/+}$ *Wapl*$^{+/+}$ and 5× *Wapl*$^{fl/+}$ mice, and the control mice in (**g**) were 2× *Rag1*$^{Cre/+}$ *Wapl*$^{+/+}$, 2× *Wapl*$^{fl/fl}$, 1× *Wapl*$^{fl/+}$ and 1× *Wapl*$^{+/+}$. Statistical data (**a**,**b**,**d**,**f**,**g)** are shown as mean values with SEM and were analysed by multiple *t*-tests (unpaired and two-tailed with Holm-Sidak correction). One of 5 (**c**) or 4 (**e**) experiments is shown. *n*, number of mice. Each dot corresponds to one mouse.

Extended Data Fig. 8 | V_H-DJ_H recombination and looping in *Wapl* mutant mice.

a, VDJ-seq analysis of *Igh* rearrangements in *Wapl*$^{\Delta P1,2/\Delta P1,2}$, *Wapl*$^{\Delta P1,2/+}$, *Wapl*$^{\Delta P1/\Delta P1}$, *Wapl*$^{\Delta P2/\Delta P2}$ and *Wapl*$^{+/+}$ pro-B cells as well as in *Pax5*$^{\Delta/\Delta}$ progenitors (*Vav*-Cre *Pax5*$^{fl/fl}$), which were performed in 4 different experimental series. The percentages of uniquely identified DJ_H and VDJ_H sequences are shown as mean values with SEM and were analysed by multiple *t*-tests (unpaired and two-tailed with Holm-Sidak correction). **b**, V_H gene recombination in *Wapl*$^{+/+}$ and mutant pro-B-cells, as determined by pairwise VDJ-seq experiments. The VDJ-seq data of *Wapl*$^{+/+}$ and mutant pro-B-cells are shown in the upper and lower part, respectively. The V_H gene usage is shown as mean percentage of all DJ_H and VDJ_H rearrangement events with SEM. **c**, *Wapl* mRNA expression in *in vitro* cultured *v-Abl* transformed pro-B cells of the wild-type (light grey) or *Rag2*$^{-/-}$ (grey) genotype as well as in *ex vivo* sorted *Wapl*$^{\Delta P1,2/\Delta P1,2}$ (blue)

and wild-type *Wapl*$^{+/+}$ (black) pro-B cells. The *Wapl* expression was determined by RT-qPCR analysis relative to the *Tbp* expression and is shown a mean value relative to that of the *Wapl*$^{+/+}$ pro-B cells (set to 1). **d**, 3C-seq analysis of interactions across the *Igh* locus from the 5' viewpoints (V_H1-83/81) in short-term cultured *Wapl*$^{\Delta P1,2/\Delta P1,2}$ *Rag2*$^{-/-}$ and *Wapl*$^{+/+}$ *Rag2*$^{-/-}$ pro-B cells. The 3C-seq reads are mapped as normalized counts. One of two experiments is show. *n*, number of experiments. Each dot corresponds to one mouse.

Extended Data Fig. 9 | Generation and analysis of conditional *Eed* mutant mice.

a, Generation of a floxed (fl) *Eed* allele. The *Eed*$^{\text{fl-Neo}}$ allele was generated by replacing exon 6 of the *Eed* gene with the following sequences in the 5' to 3' direction: (i) a *lox*P-flanked *Eed* cDNA fragment (from exon 6 to the 5' part of the 3'UTR) linked to six copies of the SV40 polyadenylation (pA) region, (ii) a DNA fragment containing the 3' splice site and 5' sequences of exon 6 fused in-frame to the coding sequence of *Gfp* followed by an SV40 pA sequence and (iii) a *frt*-flanked DNA fragment containing the mouse phosphoglycerate kinase 1 (*Pgk1*) promoter linked to the neomycin (Neo) resistance gene. Brackets indicate the two homology regions used for ES cell recombination. The *frt* (blue) and *lox*P (red) sites (arrowheads) of the *Eed*$^{\text{fl-Neo}}$ allele were used to generate the *Eed*^{fl} and *Eed*$^{\Delta}$ alleles by sequential Flpe- and Cre-mediated deletion *in vivo*. The six SV40 pA sequences downstream of the last *Eed* exon prevented RNA splicing to the *Gfp* exon prior to Cre-mediated deletion, as demonstrated by flow cytometry (**e**, right). A genotyping gel image of *Eed*$^{+/+}$, *Eed*$^{\text{fl/+}}$, and *Eed*$^{\text{fl/fl}}$ mice is shown to the right. **b**, Selective loss of H3K27me3 at the *Wapl* promoter in *Wapl*$^{\Delta P1/\Delta P1}$ pro-B cells (light blue) compared to *Wapl*$^{+/+}$ pro-B cells (black). The H3K27me3 signal is precipitously lost 220 bp upstream of the P1 site. One of two ChIP-seq experiments are shown. **c**, Loss of Ezh2 and

Pax5 binding at the *Wapl* promoter in mature B cells after two days of activation. **d**, Co-precipitation of Myc-tagged Ezh2 or IRF4 by streptavidin (SA) pulldown of biotinylated Pax5-Bio from nuclear extracts prepared from HEK-293T cells that were transiently transfected with expression vectors encoding Pax5-Bio-IRES-BirA, Myc-Ezh2, Eed and Suz12 or Pax5-Bio-IRES-BirA and Myc-IRF4. The input (1/100) and protein precipitates were analysed by immunoblotting with antibodies detecting Myc and Pax5. The band indicated by an asterisk may correspond to endogenous Myc. One of four experiments is shown with marker proteins (kilodaltons). **e**, Flow cytometric analysis of bone marrow from *Rag1*$^{Cre/+}$ *Eed*$^{fl/fl}$ (blue) and control (black) mice. *Rag1*$^{Cre/+}$ *Eed*$^{fl/+}$, *Rag1*$^{Cre/+}$, *Eed*$^{fl/+}$ and *Eed*$^{+/+}$ mice were used as control. The relative frequencies of the indicated cell types (left), which were determined in six experiments, are shown as mean values with SEM and were analysed by multiple *t*-tests (unpaired and two-tailed with Holm-Sidak correction). GFP expression (right) is shown for *Rag1*$^{Cre/+}$ *Eed*$^{fl/fl}$ pro-B cells in contrast to control *Eed*$^{fl/+}$ pro-B cells. **f**, Scatterplot of gene expression differences between Eed-deficient and control pro-B cells. Eed-activated (blue) and Eed-repressed (red) genes were defined by an expression difference of > 3-fold, an adjusted *P* value of < 0.05 and a TPM value of > 5 in Eed-deficient or control pro-B cells, respectively (Supplementary Table 2). The expression data are based on 5 (*Rag1*$^{Cre/+}$ *Eed*$^{fl/fl}$) and 4 (control; 3× *Rag1*$^{Cre/+}$ *Eed*$^{fl/+}$, 1× *Eed*$^{fl/fl}$) RNA-seq experiments. **g**, Functional classification and quantification of the proteins encoded by Eed-activated and Eed-repressed genes (Supplementary Table 2). The bar size indicates the percentage of activated or repressed genes in each functional class relative to the total activated or repressed genes, respectively. Numbers in the bars refer to the genes in each functional class. **h**, Expression of selected genes in Eed-deficient (grey) and Eed-expressing (black) pro-B cells. The expression of the indicated genes, which are not differentially expressed according to the definition in **f**, is shown as mean TPM value with SEM.

i,**j**, VDJ-seq analysis of *Rag1*$^{Cre/+}$ *Eed*$^{fl/fl}$ and control pro-B cells. **i**, The mean percentages of uniquely identified DJ_H and VDJ_H sequences were determined based on 4 (*Rag1*$^{Cre/+}$ *Eed*$^{fl/fl}$) and 2 (control; 1× *Eed*$^{fl/+}$, 1× *Eed*$^{+/+}$) experiments. **j**, The V_H gene usage is shown as mean percentage of all VDJ_H rearrangement events with SEM. *n*, number of experiments. Each dot corresponds to one mouse (**e**,**h**,**i**) or one gene (**f**).

Extended Data Fig. 10 | Changes of chromosomal architecture and gene expression in *Wapl*$^{+/+}$ and *Wapl*$^{\Delta P1,2/\Delta P1,2}$ pro-B cells. a, iFRAP analysis of splenic mature B cells from *Wapl*$^{\Delta P1,2/+}$ (blue) and *Wapl*$^{+/+}$ (pink) mice carrying the *Smc3-Gfp* transgene. The difference in fluorescence intensity between bleached and unbleached regions is plotted against time. The mean values are indicated by lines and the SD by shading. *n*, number of cells analysed in three experiments per genotype**. b**, Frequency distribution of intra-chromosomal contacts as a function of the genomic distance using logarithmically increased genomic distance bins, as determined by Homer analysis of Hi-C data generated with short-term cultured pro-B cells (grey) and *ex vivo* sorted splenic mature B cells (pink) from wild-type mice. **c**, Hi-C contact matrices of a zoomed-in region on chromosome 12 (mm9: 72,500,000-78,500,000; upper row) and 16 (21,500,000-28,500,000; lower row), displayed at a 10-kb bin resolution for *Pax5*$^{\Delta/\Delta}$ progenitors, *Wapl*$^{+/+}$ and *Wapl*$^{\Delta P1,2/\Delta P1,2}$ pro-B cells. Black dots indicate loop anchors identified with Juicebox, and the intensity of each pixel represents the normalized number of contacts between a pair of loci (Durand et al. 2016. *Cell Syst*. 3, 95-98). The maximum intensity is indicated in the lower left of each panel. **d**, Density distribution of the loop length in *Pax5*$^{\Delta/\Delta}$ progenitors, *Wapl*$^{+/+}$ and *Wapl*$^{\Delta P1,2/\Delta P1,2}$ pro-B cells, as determined with HiCCUPS of Juicer. The median loop length (in

kb) is shown for each genotype. **e**, Scatterplot of gene expression differences, based on two RNA-seq experiments per genotype. Genes upregulated (red) or downregulated (blue) in *Wapl*$^{\Delta P1,2/\Delta P1,2}$ pro-B cell compared to *Wapl*$^{+/+}$ pro-B cells were defined by an expression difference of > 2-fold, an adjusted *P* value of < 0.05 and a TPM value of > 5 in at least one of the two pro-B cell types (Supplementary Table 3). **f**, Functional classification and quantification of the proteins encoded by up-regulated (red) and down-regulated (blue) genes in *Wapl*$^{\Delta P1,2/\Delta P1,2}$ pro-B cells relative to *Wapl*$^{+/+}$ pro-B cells (Supplementary Table 3). See Extended Data Fig. 9g for detailed explanation. **g**, Expression of selected genes in *Wapl*$^{\Delta P1,2/\Delta P1,2}$ (grey) and *Wapl*$^{+/+}$ (black) pro-B cells. The expression of the indicated genes, which are not differentially expressed according to the definition in **e**, is shown as mean TPM value. **h**, Schematic diagram depicting a 'stable' loop formed by loop extrusion across the entire *Igh* locus in pro-B cells. The forward CBEs (in the V_H gene cluster and IGCR region) and the reverse CBEs (in the IGCR and 3'CBE regions) are indicated by red and blue arrows, respectively. The RAG-bound recombination centre, which is located at the DJ_H-rearranged gene segment (Ji *et al*. 2010. *Cell* 141, 419-431), is indicated in grey. The convergent orientation of the 12-RSS (recognition signal sequence with a 12-bp spacer, black arrowhead) of the D_H segment and the 23-RSS (with a 23-bp spacer, green arrowhead) of the V_H genes is essential for mediating RAG-cleavage and deletional joining (Alt *et al*. 2013. *Cell* 152, 417-429). The loop-extruding cohesin ring (orange) is arrested at convergent CBEs. In a 'stable' loop, the correct alignment of the RSS elements of a V_H gene and the DJ_H-rearranged gene segment likely occurs by local diffusion. Arrowheads symbolize the RSS element consisting of the heptamer, nonamer and intervening spacer. **i**, Correct alignment of the RSS elements of a V_H gene and the DJ_H-rearranged gene segment may be mediated by the ongoing process of loop extrusion. Orange and black arrows indicate the direction of movement of cohesin and DNA, respectively. **j**, Misalignment of the RSS elements of an inverted V_H gene

and the DJ_H-rearranged gene segment during loop extrusion, which prevents RAG-mediated cleavage.

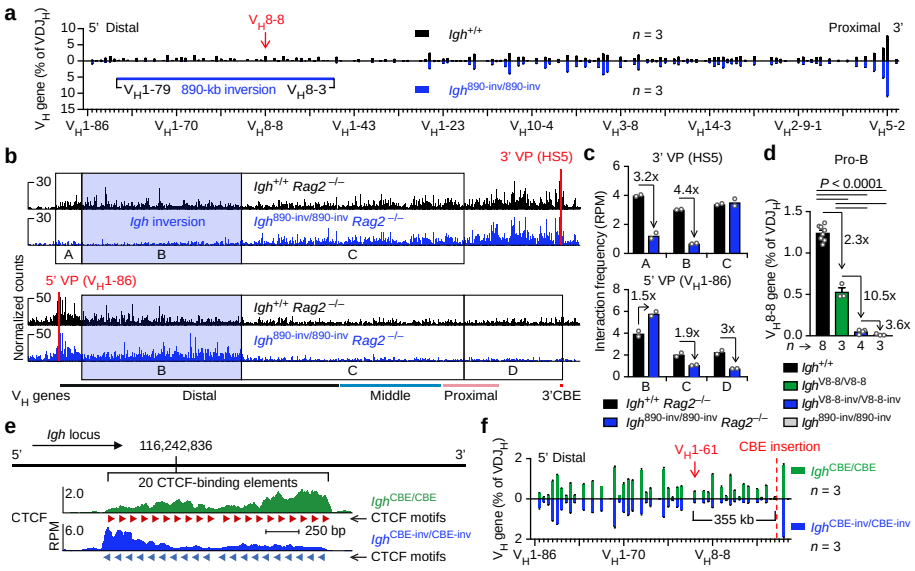

Figure 1 (Hill et al.)

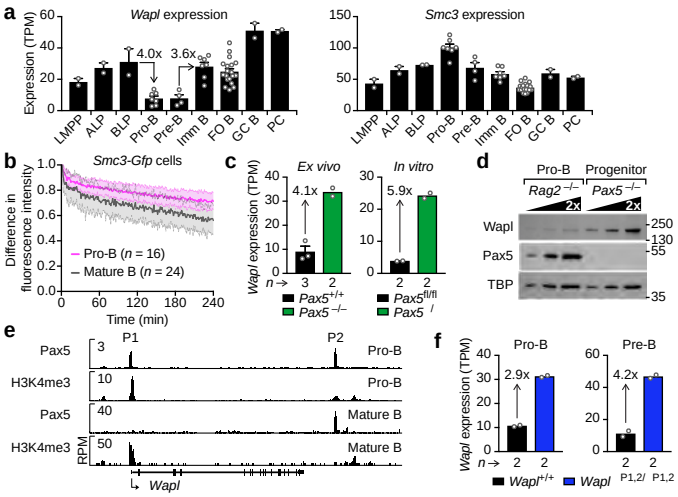

Figure 2 (Hill et al.)

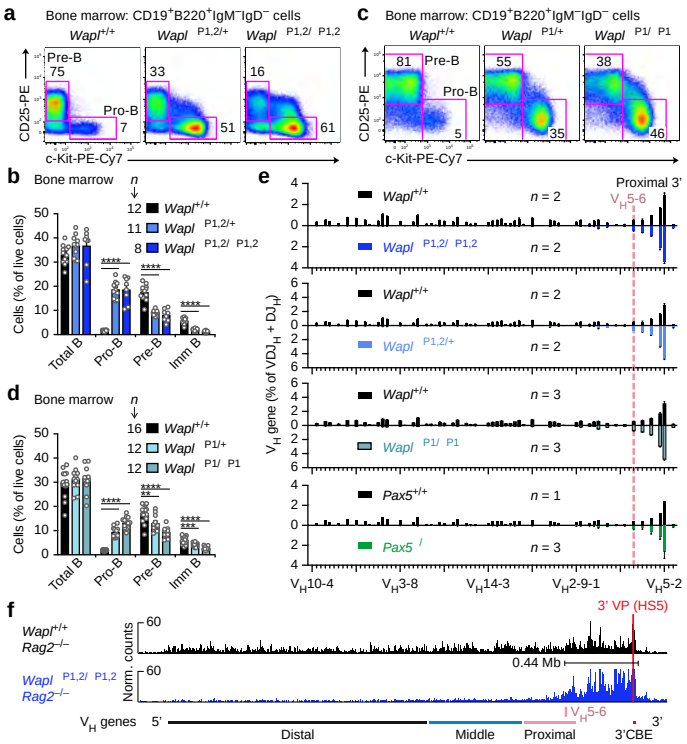

Figure 3 (Hill et al.)

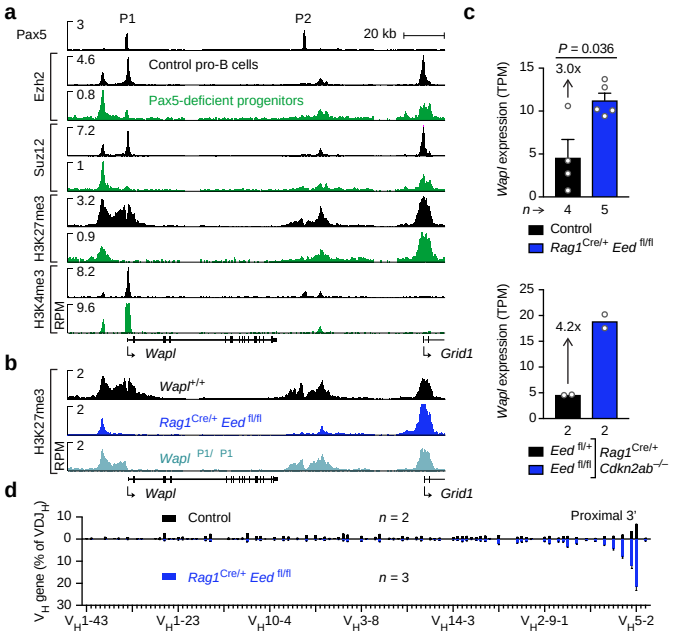

Figure 4 (Hill et al.)

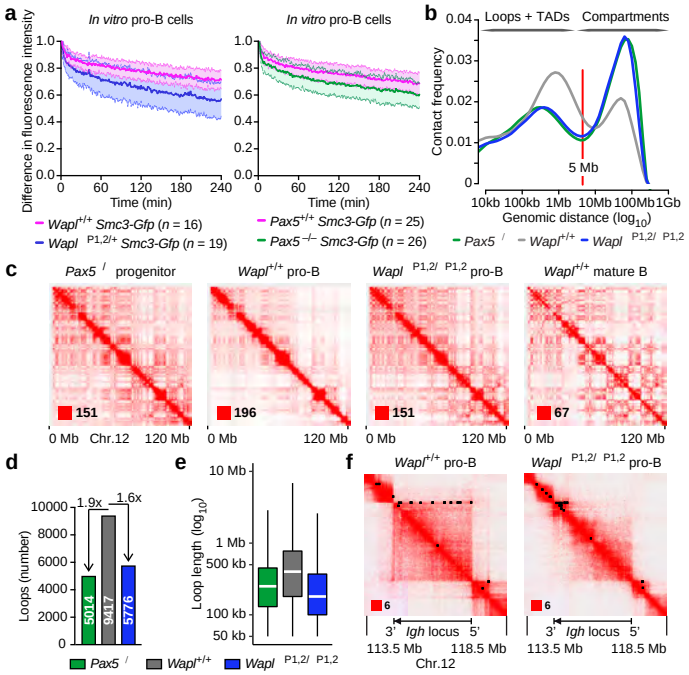

Figure 5 (Hill et al.)

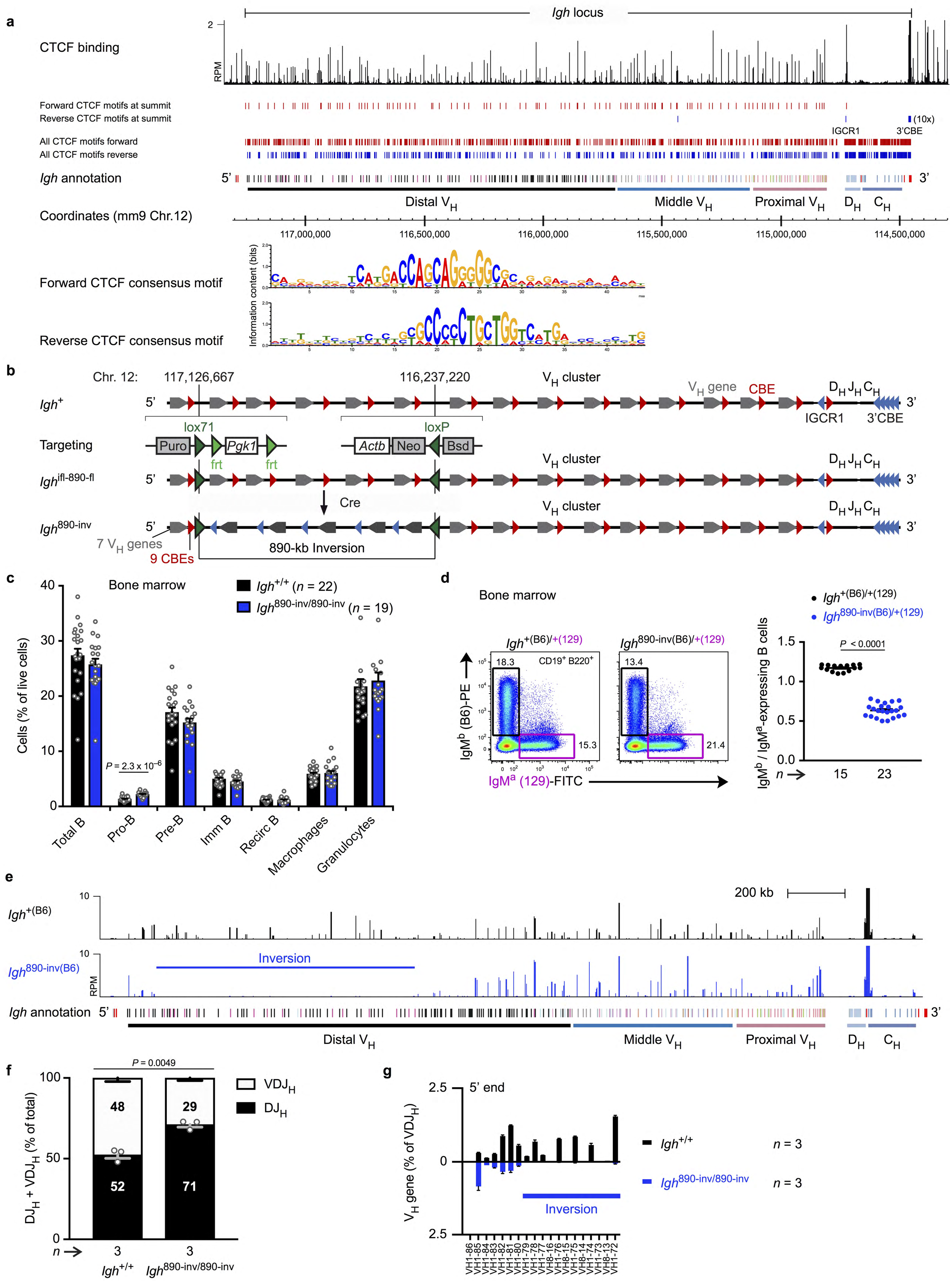
a
Igh locus
CTCF binding
RPM
Forward CTCF motifs at summit
Reverse CTCF motifs at summit
(10x)
IGCR1
3'CBE
All CTCF motifs forward
All CTCF motifs reverse
Igh annotation
5'
3'
Distal VH
Middle VH
Proximal VH
DH
CH
Coordinates (mm9 Chr.12)
117,000,000
116,500,000
116,000,000
115,500,000
115,000,000
114,500,000
Forward CTCF consensus motif
Reverse CTCF consensus motif
Information content (bits)
b
Chr. 12:
117,126,667
116,237,220
VH cluster
VH gene
CBE
DH JH CH
Igh+
IGCR1
3'CBE
lox71
loxP
Targeting
Puro
Pgk1
Actb
Neo
Bsd
frt
Igh ifl-890-fl
Cre
Igh 890-inv
7 VH genes
9 CBEs
890-kb Inversion
c
Bone marrow
Igh+/+ (n = 22)
Igh 890-inv/890-inv (n = 19)
Cells (% of live cells)
P = 2.3 x 10−6
Total B
Pro-B
Pre-B
Imm B
Recirc B
Macrophages
Granulocytes
d
Bone marrow
Igh+(B6)/+(129)
Igh 890-inv(B6)/+(129)
CD19+ B220+
18.3
15.3
13.4
21.4
IgMb (B6)-PE
IgMa (129)-FITC
IgMb / IgMa-expressing B cells
P < 0.0001
n
15
23
e
200 kb
Igh+(B6)
Igh 890-inv(B6)
Inversion
RPM
Igh annotation
Distal VH
Middle VH
Proximal VH
DH
CH
f
P = 0.0049
VDJH
DJH
DJH + VDJH (% of total)
48
52
29
71
Igh+/+
Igh 890-inv/890-inv
g
5' end
VH gene (% of VDJH)
Igh+/+
Igh 890-inv/890-inv
n = 3
n = 3
Inversion
VH1-86
VH1-85
VH1-84
VH1-83
VH1-82
VH1-81
VH1-80
VH1-79
VH1-78
VH1-77
VH8-16
VH1-76
VH8-15
VH1-75
VH8-14
VH1-74
VH1-73
VH8-13
VH1-72

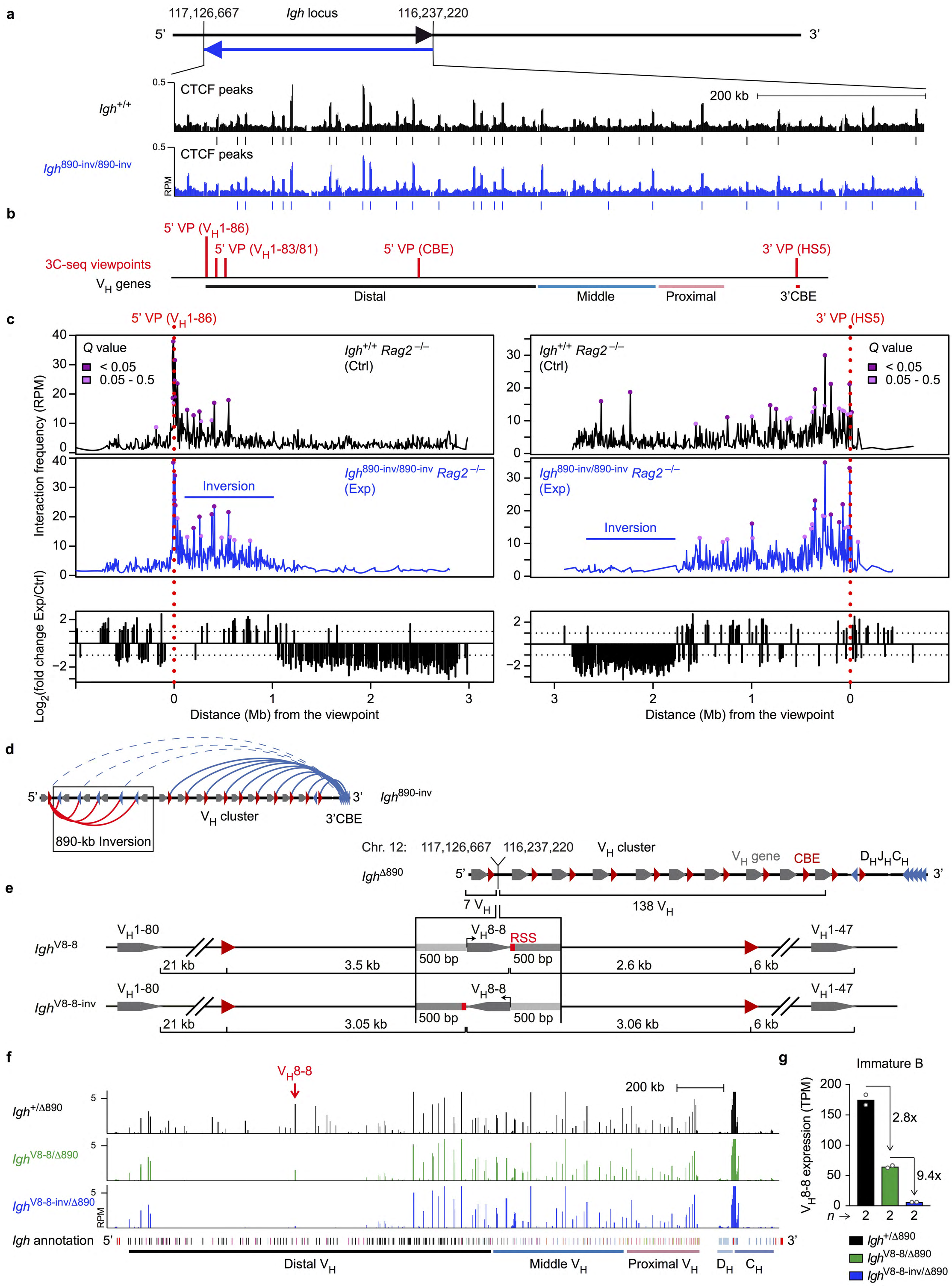
a
117,126,667
Igh locus
116,237,220
5'
3'
CTCF peaks
200 kb
Igh+/+
Igh890-inv/890-inv
RPM
b
5' VP (VH1-86)
5' VP (VH1-83/81)
5' VP (CBE)
3' VP (HS5)
3C-seq viewpoints
VH genes
Distal
Middle
Proximal
3'CBE
c
Q value
< 0.05
0.05 - 0.5
Igh+/+ Rag2−/−
(Ctrl)
Igh890-inv/890-inv Rag2−/−
(Exp)
Inversion
Interaction frequency (RPM)
Log2(fold change Exp/Ctrl)
Distance (Mb) from the viewpoint
d
890-kb Inversion
VH cluster
Igh890-inv
e
Chr. 12:
Igh∆890
VH gene
CBE
DHJHCH
7 VH
138 VH
IghV8-8
IghV8-8-inv
VH1-80
VH8-8
RSS
VH1-47
21 kb
3.5 kb
500 bp
2.6 kb
6 kb
3.05 kb
3.06 kb
f
VH8-8
Igh+/∆890
IghV8-8/∆890
IghV8-8-inv/∆890
Igh annotation
Distal VH
Middle VH
Proximal VH
DH
CH
g
Immature B
VH8-8 expression (TPM)
2.8x
9.4x
n →
Igh+/∆890
IghV8-8/∆890
IghV8-8-inv/∆890

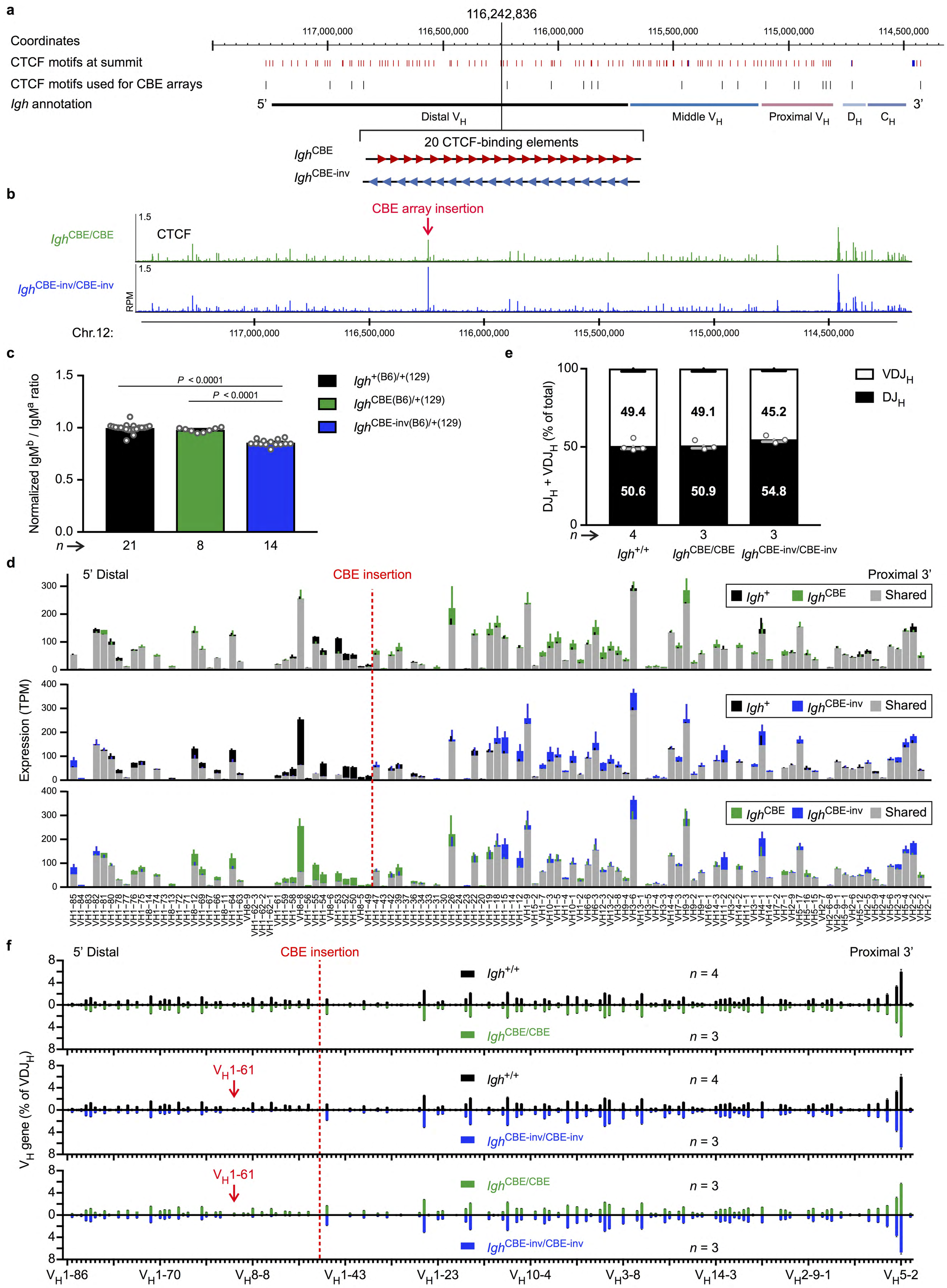
a
116,242,836
Coordinates
CTCF motifs at summit
CTCF motifs used for CBE arrays
Igh annotation
5'
3'
Distal VH
Middle VH
Proximal VH
DH
CH
20 CTCF-binding elements
IghCBE
IghCBE-inv
b
CBE array insertion
IghCBE/CBE
IghCBE-inv/CBE-inv
CTCF
RPM
Chr.12:
c
Normalized IgMb / IgMa ratio
P < 0.0001
P < 0.0001
Igh+(B6)/+(129)
IghCBE(B6)/+(129)
IghCBE-inv(B6)/+(129)
n
21
8
14
e
DJH + VDJH (% of total)
VDJH
DJH
49.4
49.1
45.2
50.6
50.9
54.8
n
4
3
3
Igh+/+
IghCBE/CBE
IghCBE-inv/CBE-inv
d
5' Distal
CBE insertion
Proximal 3'
Expression (TPM)
Igh+
IghCBE
IghCBE-inv
Shared
f
5' Distal
CBE insertion
Proximal 3'
Igh+/+
IghCBE/CBE
IghCBE-inv/CBE-inv
n = 4
n = 3
VH1-61
VH1-86
VH1-70
VH8-8
VH1-43
VH1-23
VH10-4
VH3-8
VH14-3
VH2-9-1
VH5-2
VH gene (% of VDJH)

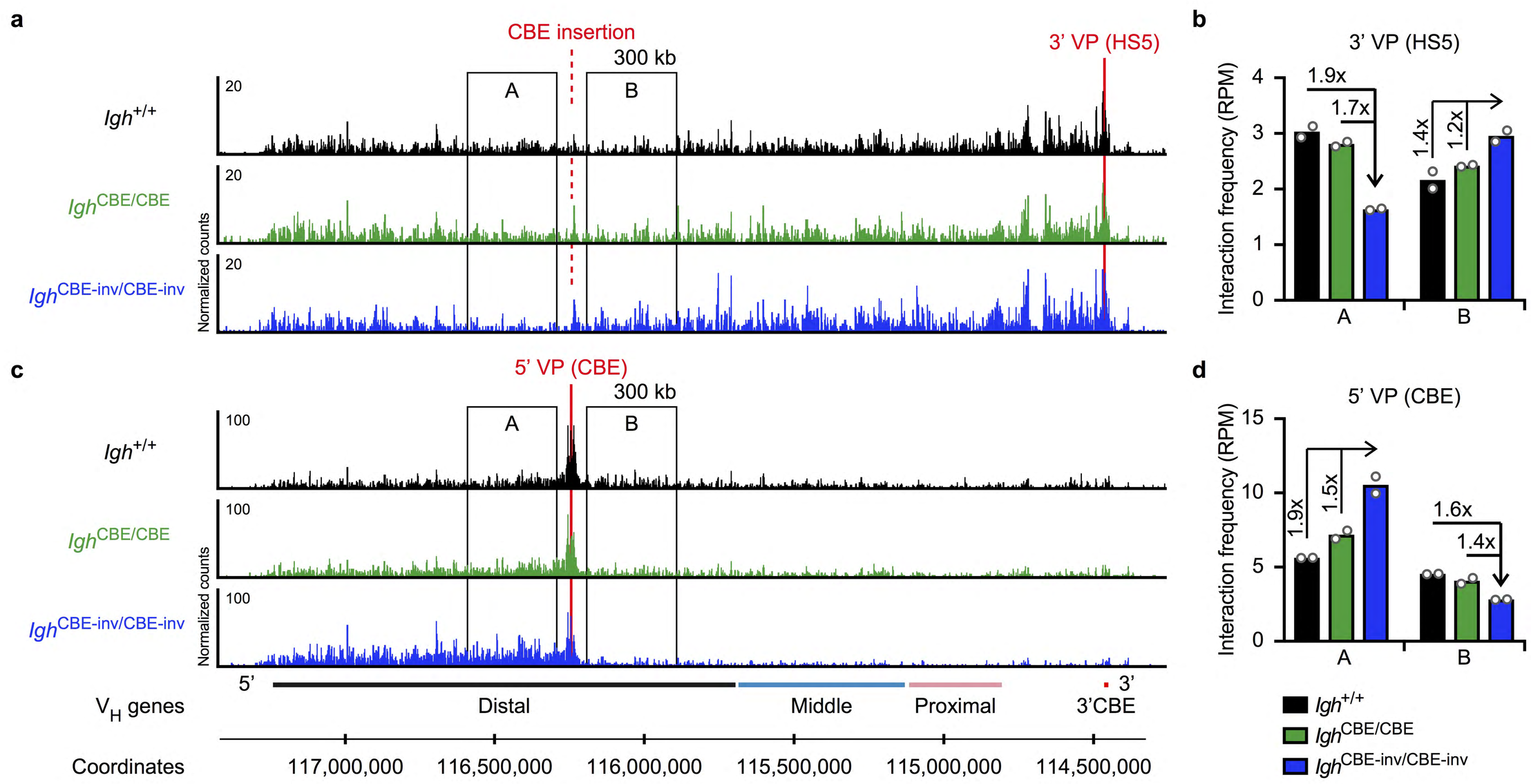
a
CBE insertion
3' VP (HS5)
300 kb
A
B
Igh+/+
IghCBE/CBE
IghCBE-inv/CBE-inv
Normalized counts
b
3' VP (HS5)
Interaction frequency (RPM)
1.9x
1.7x
1.4x
1.2x
c
5' VP (CBE)
d
1.9x
1.5x
1.6x
1.4x
VH genes
Distal
Middle
Proximal
3'CBE
Coordinates
117,000,000
116,500,000
116,000,000
115,500,000
115,000,000
114,500,000

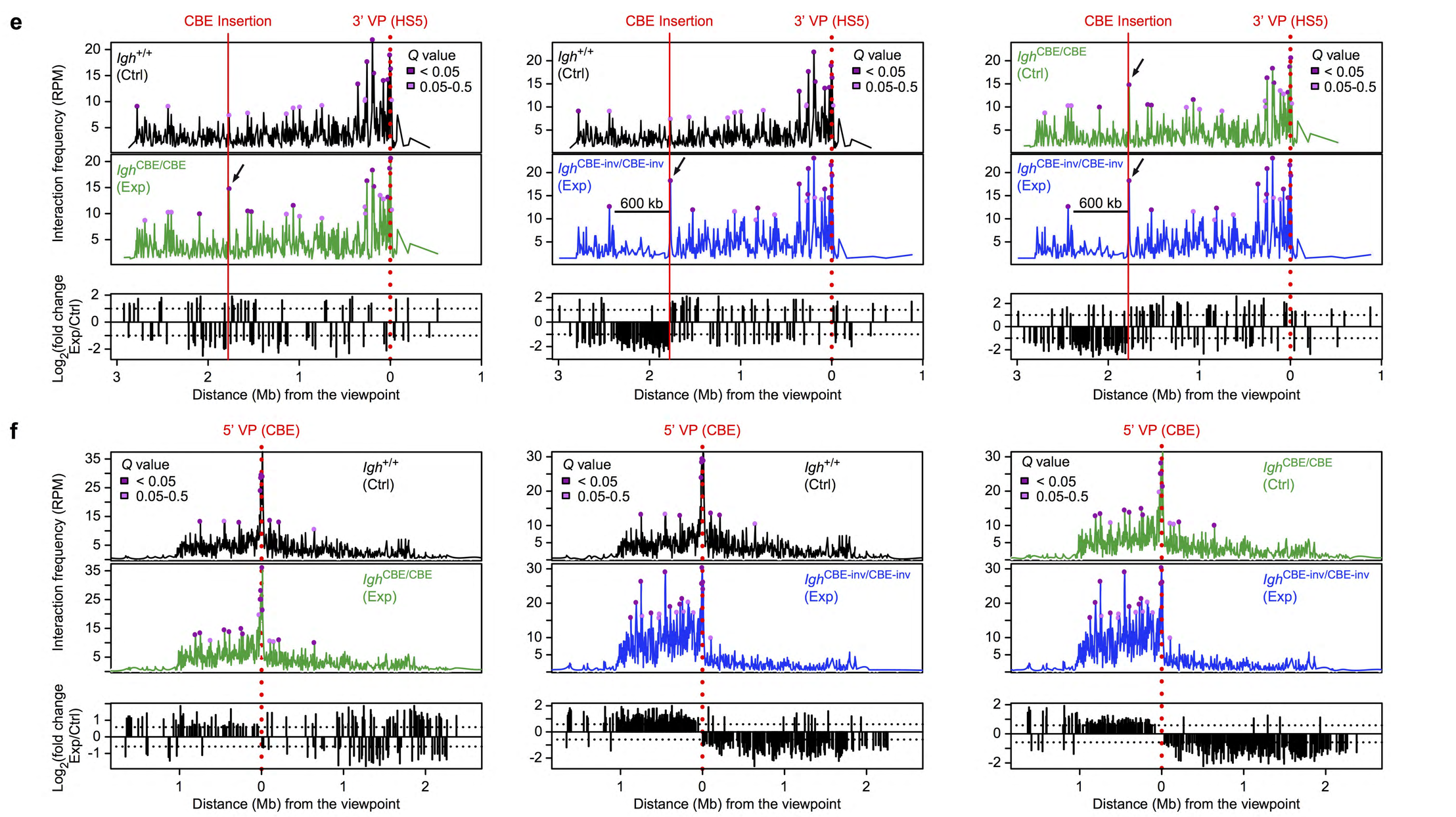
e
CBE Insertion
3' VP (HS5)
Q value
< 0.05
0.05-0.5
Igh+/+ (Ctrl)
IghCBE/CBE (Exp)
IghCBE-inv/CBE-inv (Exp)
600 kb
Interaction frequency (RPM)
Log2(fold change Exp/Ctrl)
Distance (Mb) from the viewpoint
f
5' VP (CBE)

g
5'
3'
VH cluster
3'CBE
Insertion inverted CBE array
IghCBE-inv/CBE-inv

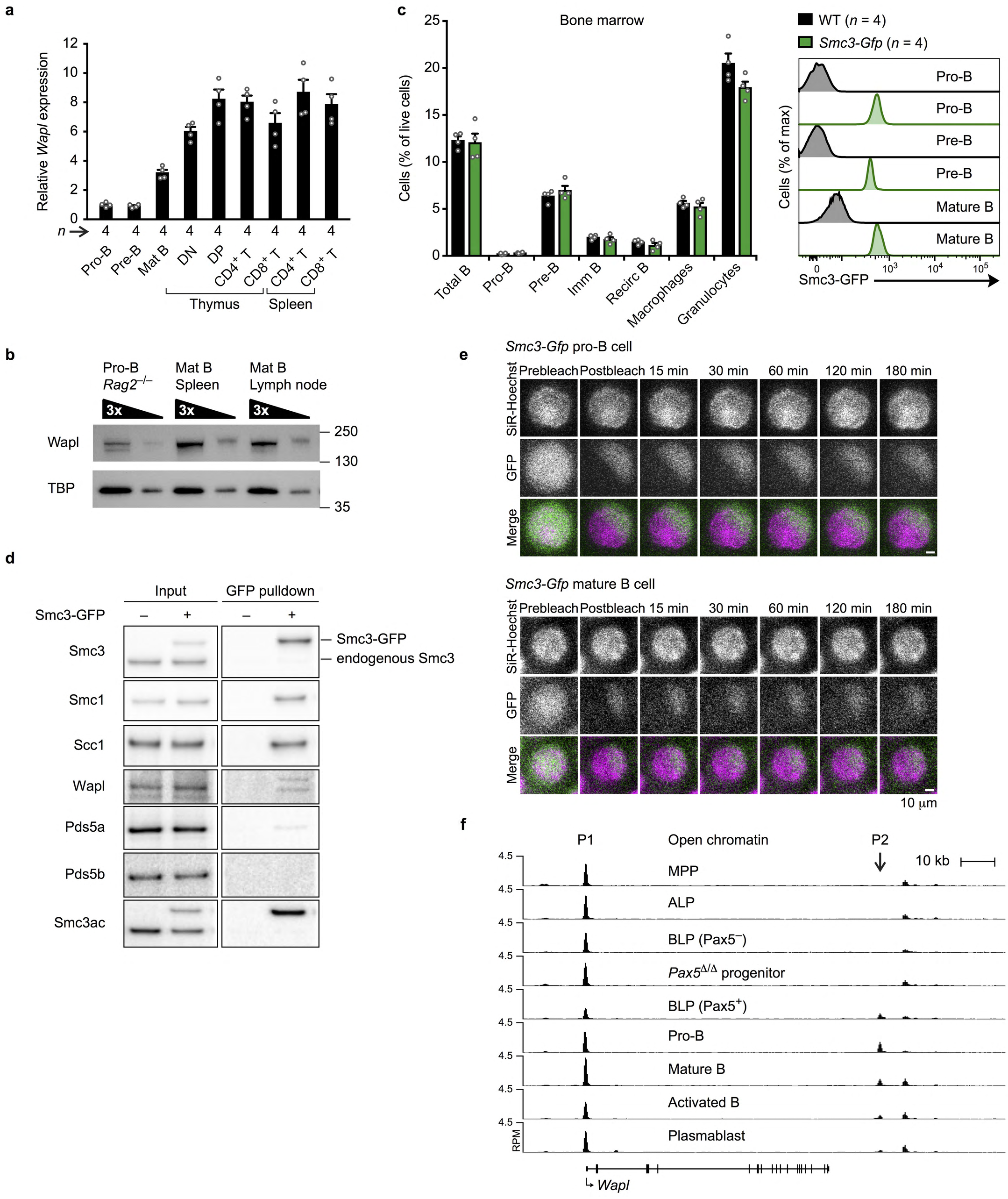
a
Relative Wapl expression
n
Pro-B
Pre-B
Mat B
DN
DP
CD4+ T
CD8+ T
CD4+ T
CD8+ T
Thymus
Spleen
b
Pro-B Rag2−/−
Mat B Spleen
Mat B Lymph node
3x
Wapl
TBP
250
130
35
c
Bone marrow
Cells (% of live cells)
Total B
Pro-B
Pre-B
Imm B
Recirc B
Macrophages
Granulocytes
WT (n = 4)
Smc3-Gfp (n = 4)
Cells (% of max)
Smc3-GFP
d
Input
GFP pulldown
Smc3-GFP
Smc3
Smc1
Scc1
Wapl
Pds5a
Pds5b
Smc3ac
Smc3-GFP
endogenous Smc3
e
Smc3-Gfp pro-B cell
Prebleach
Postbleach
15 min
30 min
60 min
120 min
180 min
SiR-Hoechst
GFP
Merge
Smc3-Gfp mature B cell
10 μm
f
P1
Open chromatin
P2
10 kb
MPP
ALP
BLP (Pax5−)
Pax5Δ/Δ progenitor
BLP (Pax5+)
Pro-B
Mature B
Activated B
Plasmablast
RPM
Wapl

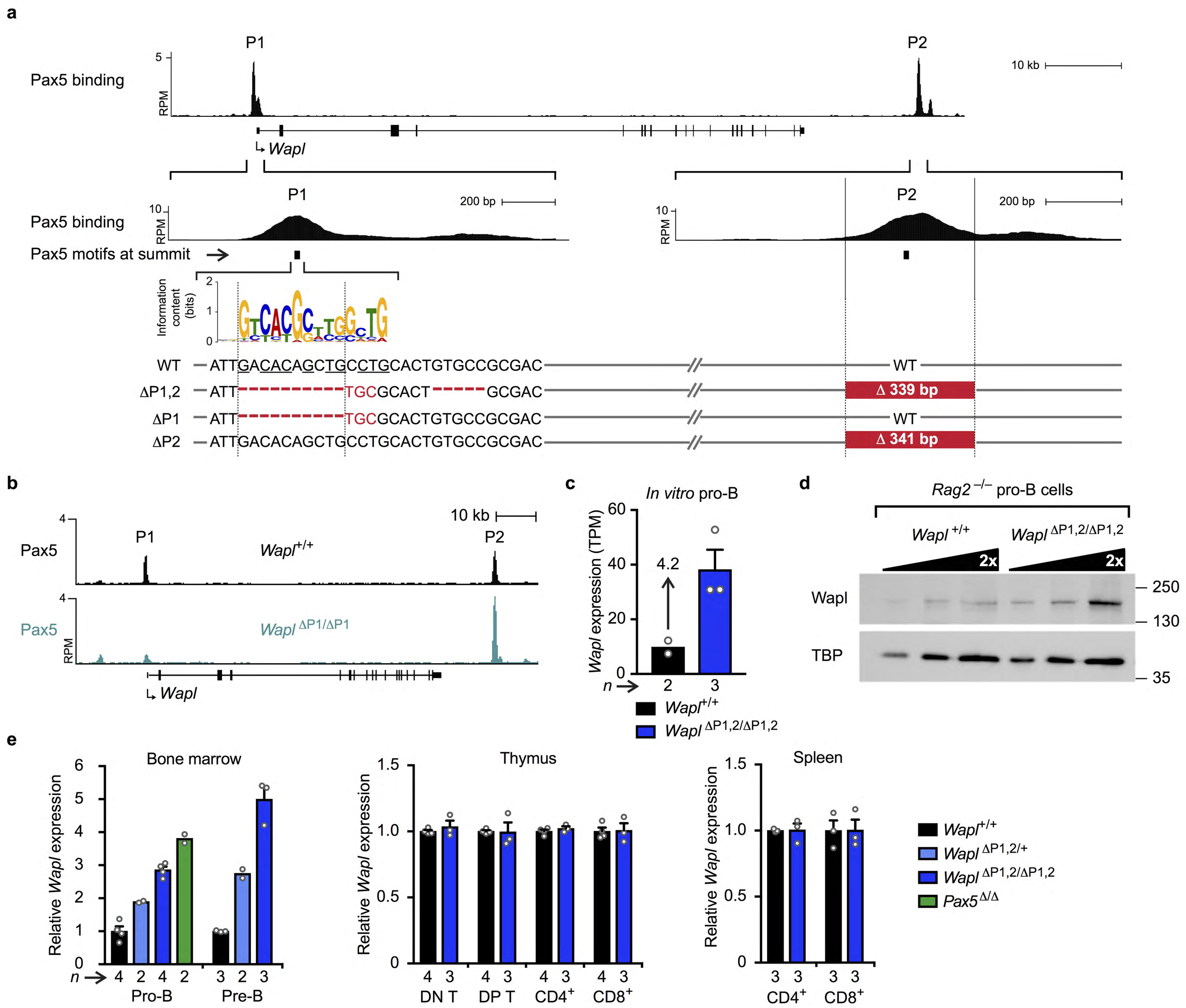
a
P1
P2
Pax5 binding
RPM
10 kb
Wapl
200 bp
Pax5 motifs at summit
Information content (bits)
WT ATTGACACAGCTGCCTGCACTGTGCCGCGAC
ΔP1,2 ATT TGCGCACT GCGAC
ΔP1 ATT TGCGCACTGTGCCGCGAC
ΔP2 ATTGACACAGCTGCCTGCACTGTGCCGCGAC
Δ 339 bp
Δ 341 bp
b
Pax5
Wapl+/+
Wapl ΔP1/ΔP1
c
In vitro pro-B
Wapl expression (TPM)
4.2
n
Wapl+/+
Wapl ΔP1,2/ΔP1,2
d
Rag2 −/− pro-B cells
Wapl +/+
Wapl ΔP1,2/ΔP1,2
2x
Wapl
TBP
250
130
35
e
Bone marrow
Thymus
Spleen
Relative Wapl expression
Pro-B
Pre-B
DN T
DP T
CD4+
CD8+
Wapl+/+
Wapl ΔP1,2/+
Wapl ΔP1,2/ΔP1,2
Pax5Δ/Δ

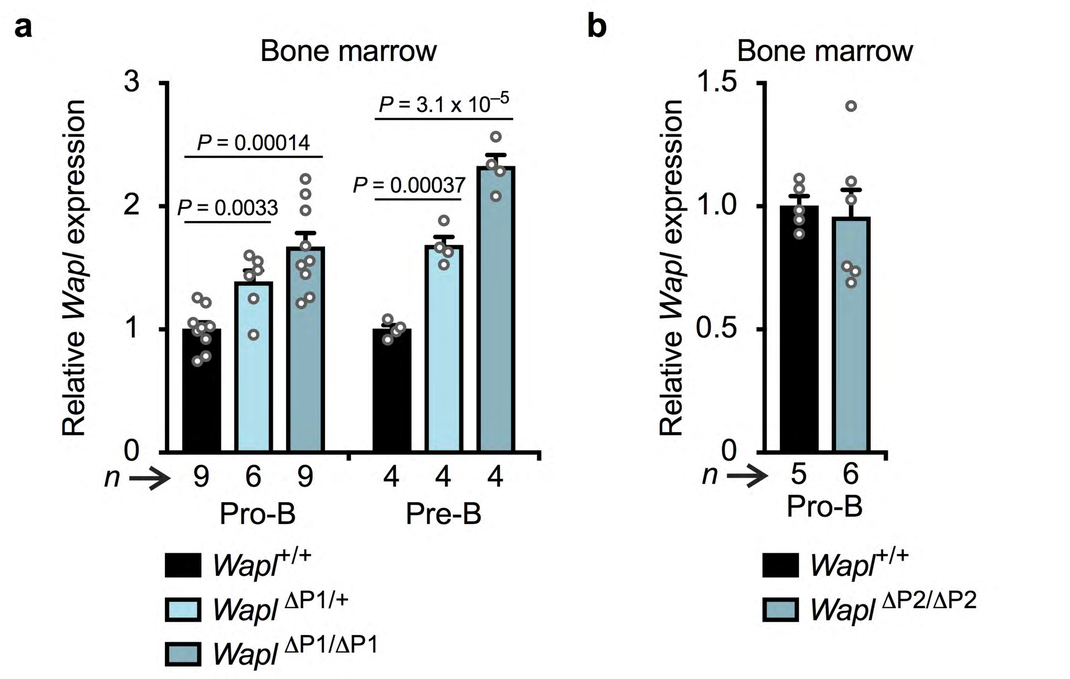
a
Bone marrow
Relative Wapl expression
P = 0.00014
P = 0.0033
P = 3.1 x 10−5
P = 0.00037
n
9 6 9
4 4 4
Pro-B
Pre-B
Wapl+/+
Wapl ΔP1/+
Wapl ΔP1/ΔP1
b
Bone marrow
Relative Wapl expression
n
5 6
Pro-B
Wapl+/+
Wapl ΔP2/ΔP2

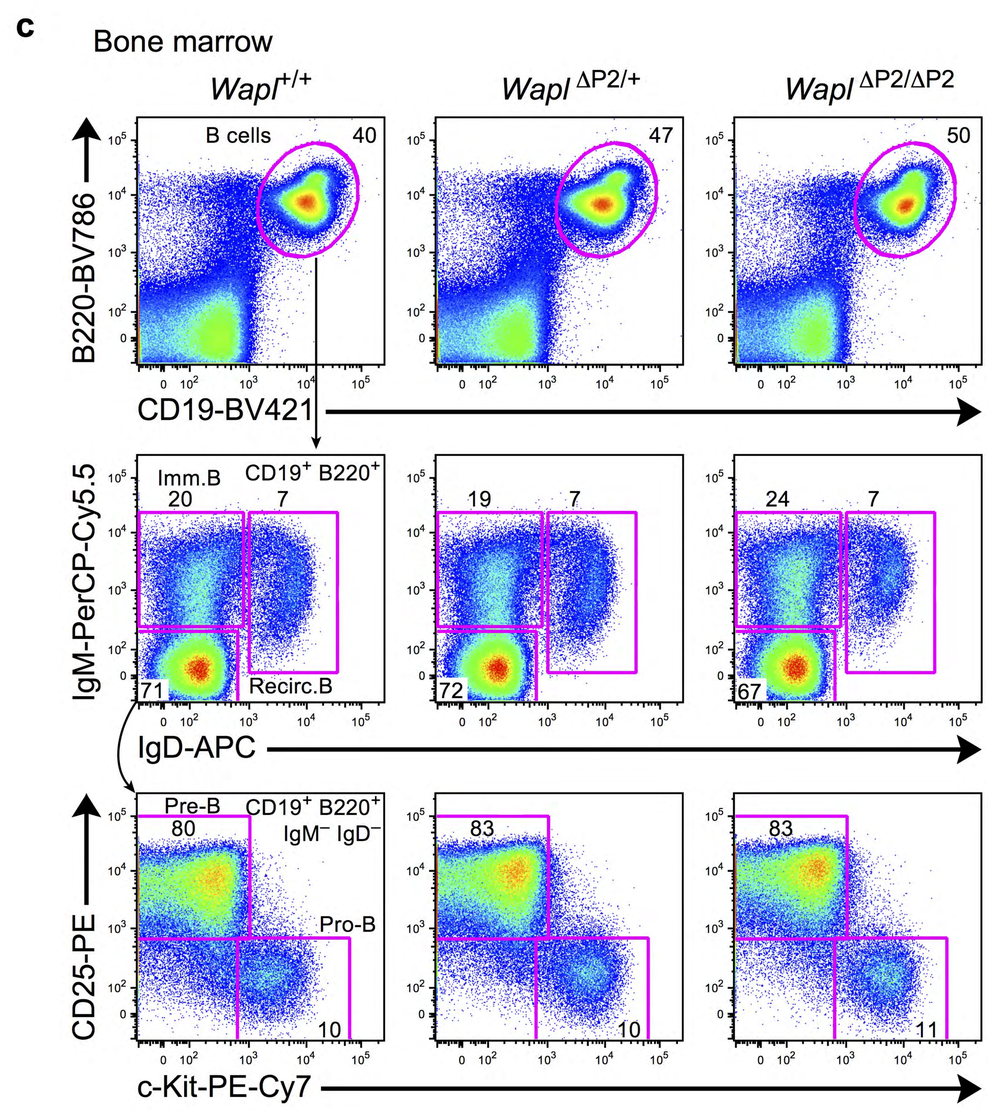
c
Bone marrow
Wapl+/+
Wapl ΔP2/+
Wapl ΔP2/ΔP2
B220-BV786
CD19-BV421
B cells
40
47
50
IgM-PerCP-Cy5.5
IgD-APC
Imm.B
20
CD19+ B220+
7
19
7
24
7
Recirc.B
71
72
67
CD25-PE
c-Kit-PE-Cy7
Pre-B
80
CD19+ B220+
IgM− IgD−
Pro-B
10
83
10
83
11

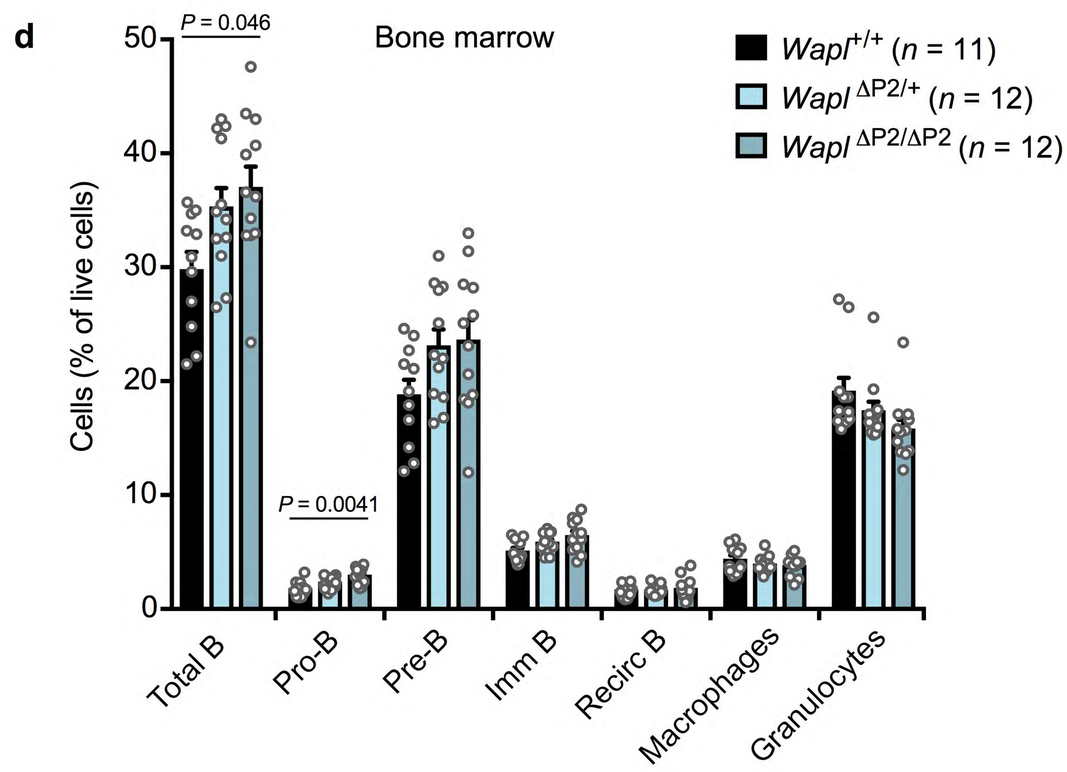
d
Bone marrow
Cells (% of live cells)
P = 0.046
P = 0.0041
Wapl+/+ (n = 11)
Wapl ΔP2/+ (n = 12)
Wapl ΔP2/ΔP2 (n = 12)
Total B
Pro-B
Pre-B
Imm B
Recirc B
Macrophages
Granulocytes

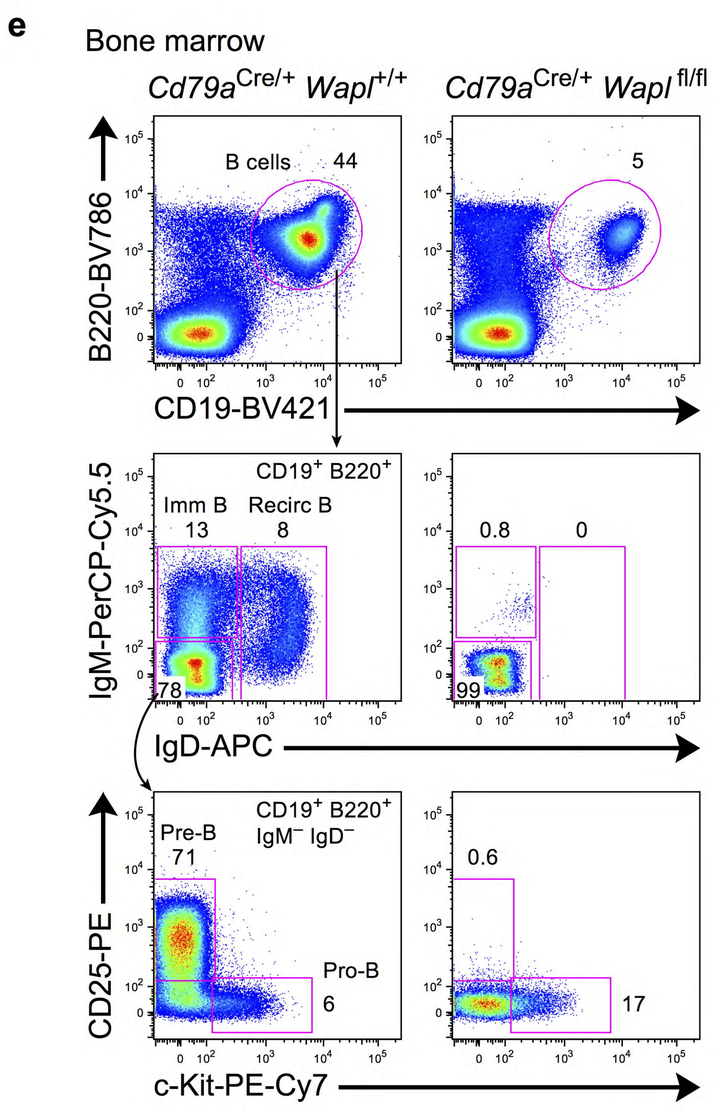
e
Bone marrow
Cd79aCre/+ Wapl+/+
Cd79aCre/+ Wapl fl/fl
B220-BV786
CD19-BV421
B cells
44
5
IgM-PerCP-Cy5.5
IgD-APC
CD19+ B220+
Imm B
13
Recirc B
8
0.8
0
78
99
CD25-PE
c-Kit-PE-Cy7
CD19+ B220+
IgM− IgD−
Pre-B
71
Pro-B
6
0.6
17

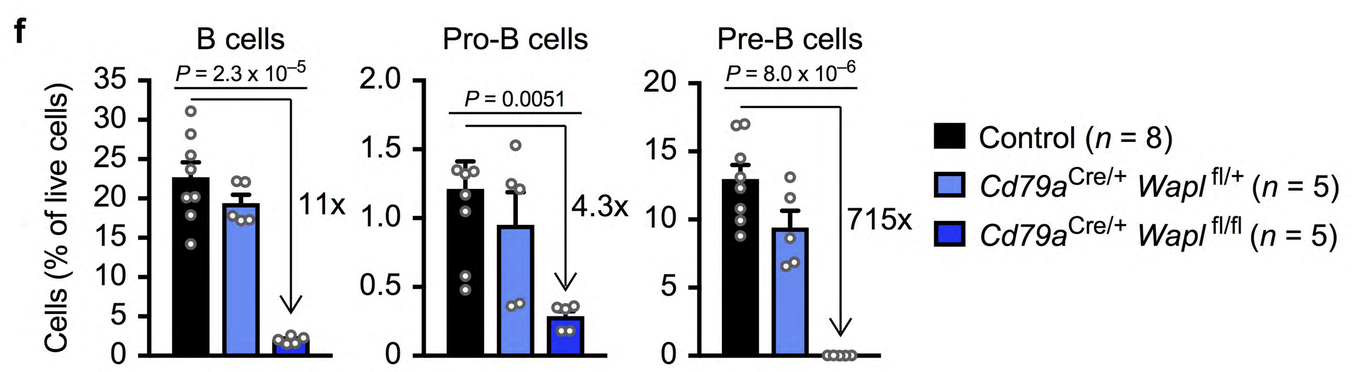
f
B cells
Pro-B cells
Pre-B cells
Cells (% of live cells)
P = 2.3 x 10−5
P = 0.0051
P = 8.0 x 10−6
11x
4.3x
715x
Control (n = 8)
Cd79aCre/+ Wapl fl/+ (n = 5)
Cd79aCre/+ Wapl fl/fl (n = 5)

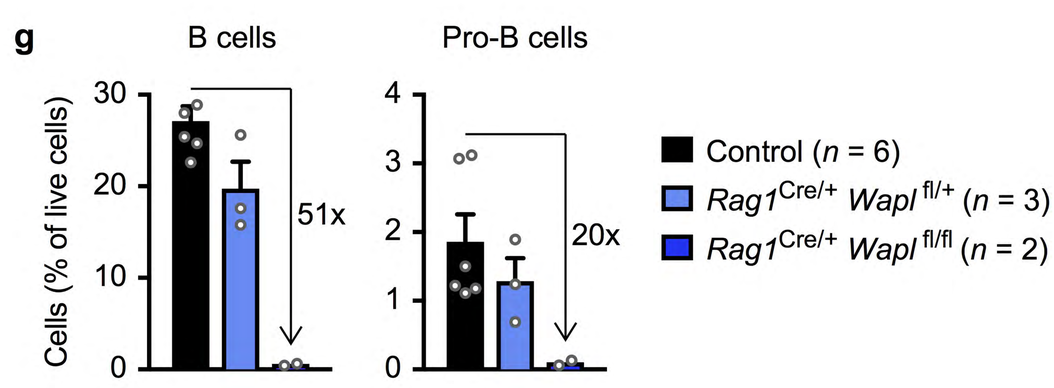
g
B cells
Pro-B cells
Cells (% of live cells)
51x
20x
Control (n = 6)
Rag1Cre/+ Wapl fl/+ (n = 3)
Rag1Cre/+ Wapl fl/fl (n = 2)

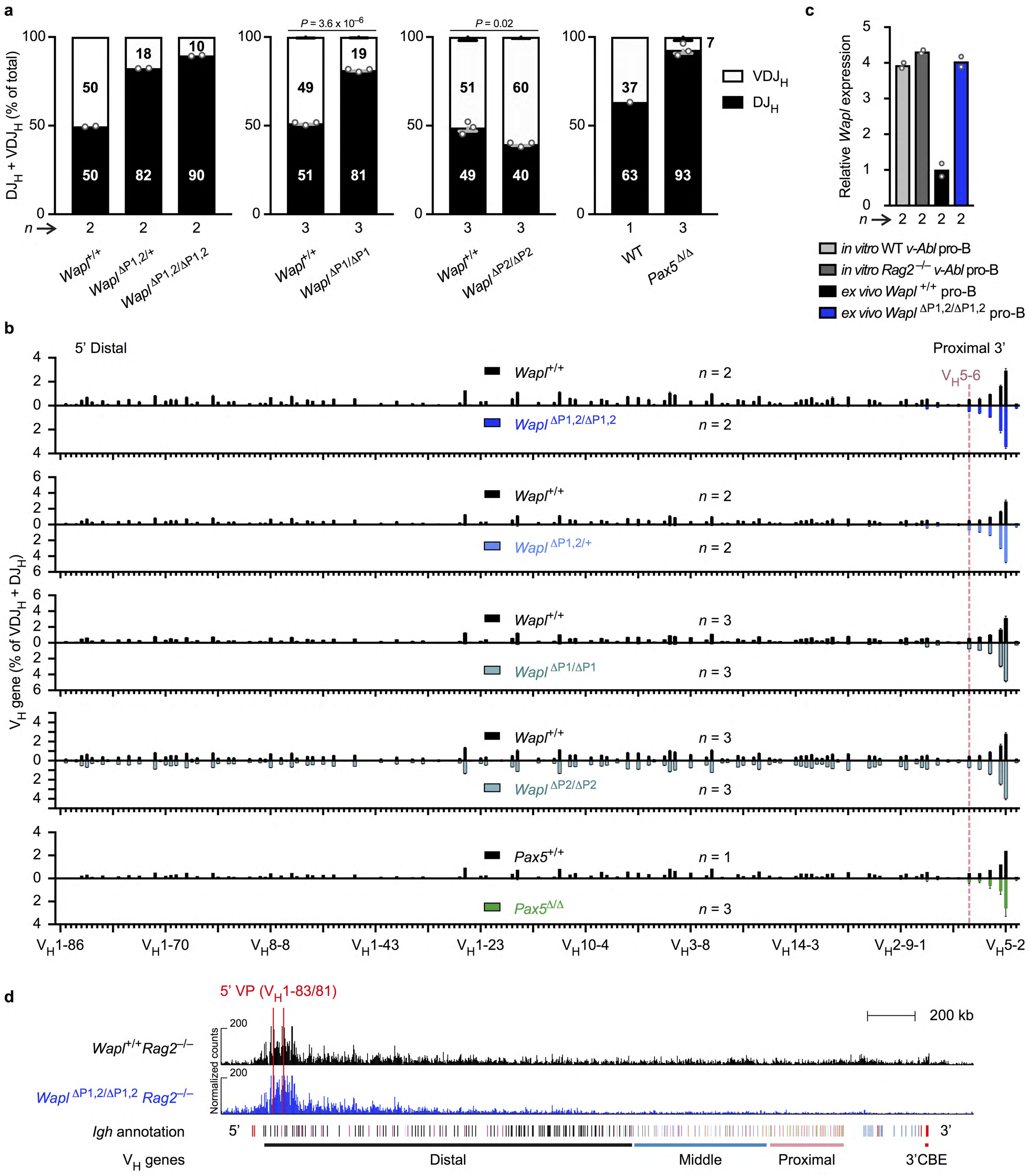
a
DJH + VDJH (% of total)
P = 3.6 x 10−6
P = 0.02
VDJH
DJH
Wapl+/+
Wapl ΔP1,2/+
Wapl ΔP1,2/ΔP1,2
Wapl ΔP1/ΔP1
Wapl ΔP2/ΔP2
WT
Pax5Δ/Δ
c
Relative Wapl expression
in vitro WT v-Abl pro-B
in vitro Rag2−/− v-Abl pro-B
ex vivo Wapl +/+ pro-B
ex vivo Wapl ΔP1,2/ΔP1,2 pro-B
b
5' Distal
Proximal 3'
VH5-6
VH gene (% of VDJH + DJH)
VH1-86
VH1-70
VH8-8
VH1-43
VH1-23
VH10-4
VH3-8
VH14-3
VH2-9-1
VH5-2
d
5' VP (VH1-83/81)
200 kb
Normalized counts
Wapl+/+Rag2−/−
Wapl ΔP1,2/ΔP1,2 Rag2−/−
Igh annotation
VH genes
Distal
Middle
Proximal
3'CBE

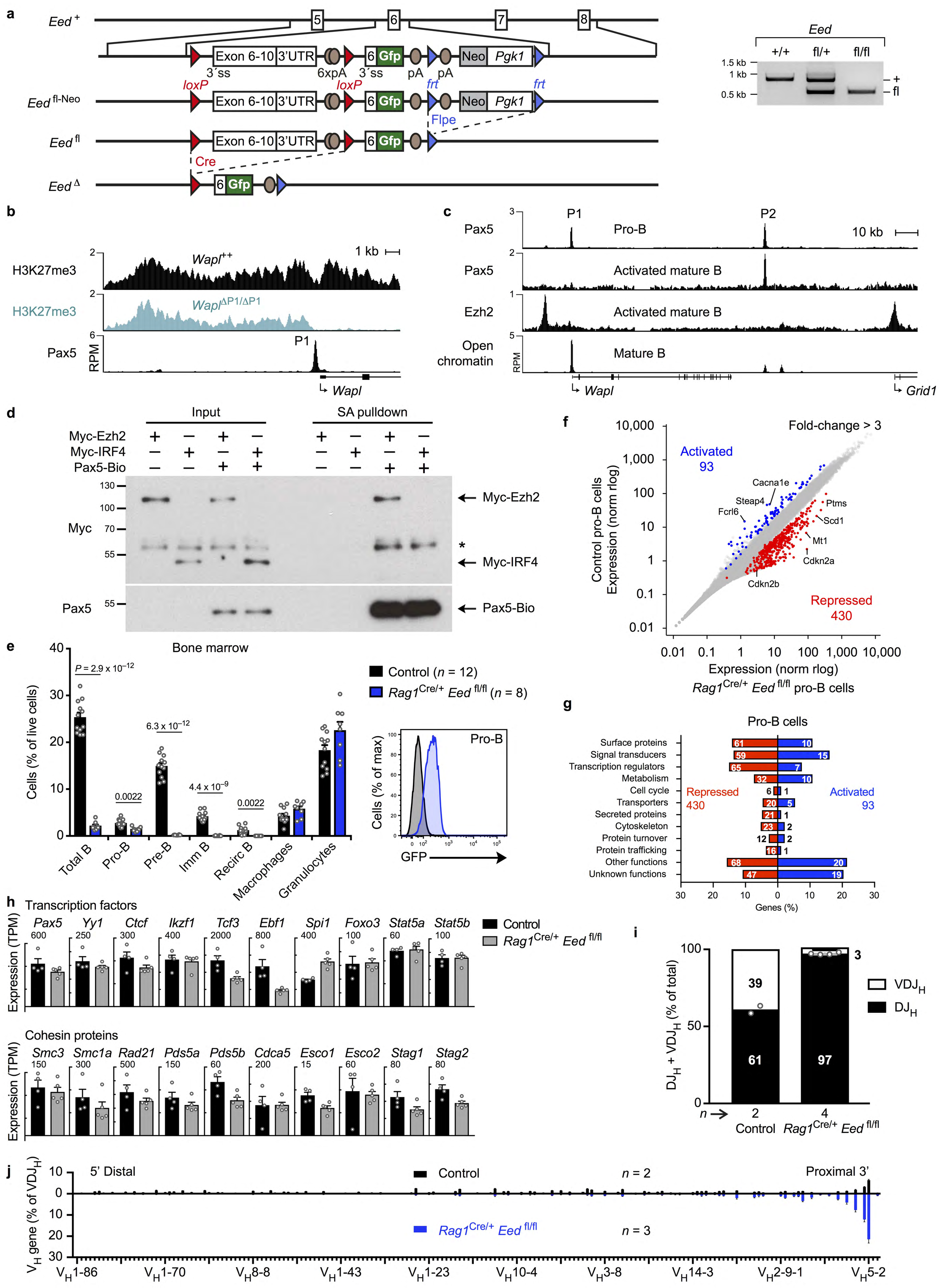
a
Eed +
Exon 6-10
3'UTR
6 Gfp
Neo
Pgk1
3´ss
6xpA
pA
loxP
frt
Eed fl-Neo
Flpe
Eed fl
Cre
Eed Δ
Eed
+/+
fl/+
fl/fl
1.5 kb
1 kb
0.5 kb
b
H3K27me3
Wapl++
1 kb
Wapl ΔP1/ΔP1
Pax5
RPM
P1
Wapl
c
P1
P2
Pro-B
10 kb
Activated mature B
Ezh2
Open chromatin
Mature B
Grid1
d
Input
SA pulldown
Myc-Ezh2
Myc-IRF4
Pax5-Bio
Myc
Pax5
Bone marrow
e
P = 2.9 x 10−12
6.3 x 10−12
0.0022
4.4 x 10−9
0.0022
Cells (% of live cells)
Total B
Pro-B
Pre-B
Imm B
Recirc B
Macrophages
Granulocytes
Control (n = 12)
Rag1Cre/+ Eed fl/fl (n = 8)
Cells (% of max)
GFP
f
Fold-change > 3
Activated
93
Repressed
430
Control pro-B cells Expression (norm rlog)
Expression (norm rlog)
Rag1Cre/+ Eed fl/fl pro-B cells
g
Pro-B cells
Surface proteins
Signal transducers
Transcription regulators
Metabolism
Cell cycle
Transporters
Secreted proteins
Cytoskeleton
Protein turnover
Protein trafficking
Other functions
Unknown functions
Genes (%)
h
Transcription factors
Pax5
Yy1
Ctcf
Ikzf1
Tcf3
Ebf1
Spi1
Foxo3
Stat5a
Stat5b
Control
Rag1Cre/+ Eed fl/fl
Expression (TPM)
Cohesin proteins
Smc3
Smc1a
Rad21
Pds5a
Pds5b
Cdca5
Esco1
Esco2
Stag1
Stag2
i
DJH + VDJH (% of total)
VDJH
DJH
Control
Rag1Cre/+ Eed fl/fl
j
5' Distal
Proximal 3'
n = 2
n = 3
VH gene (% of VDJH)
VH1-86
VH1-70
VH8-8
VH1-43
VH1-23
VH10-4
VH3-8
VH14-3
VH2-9-1
VH5-2

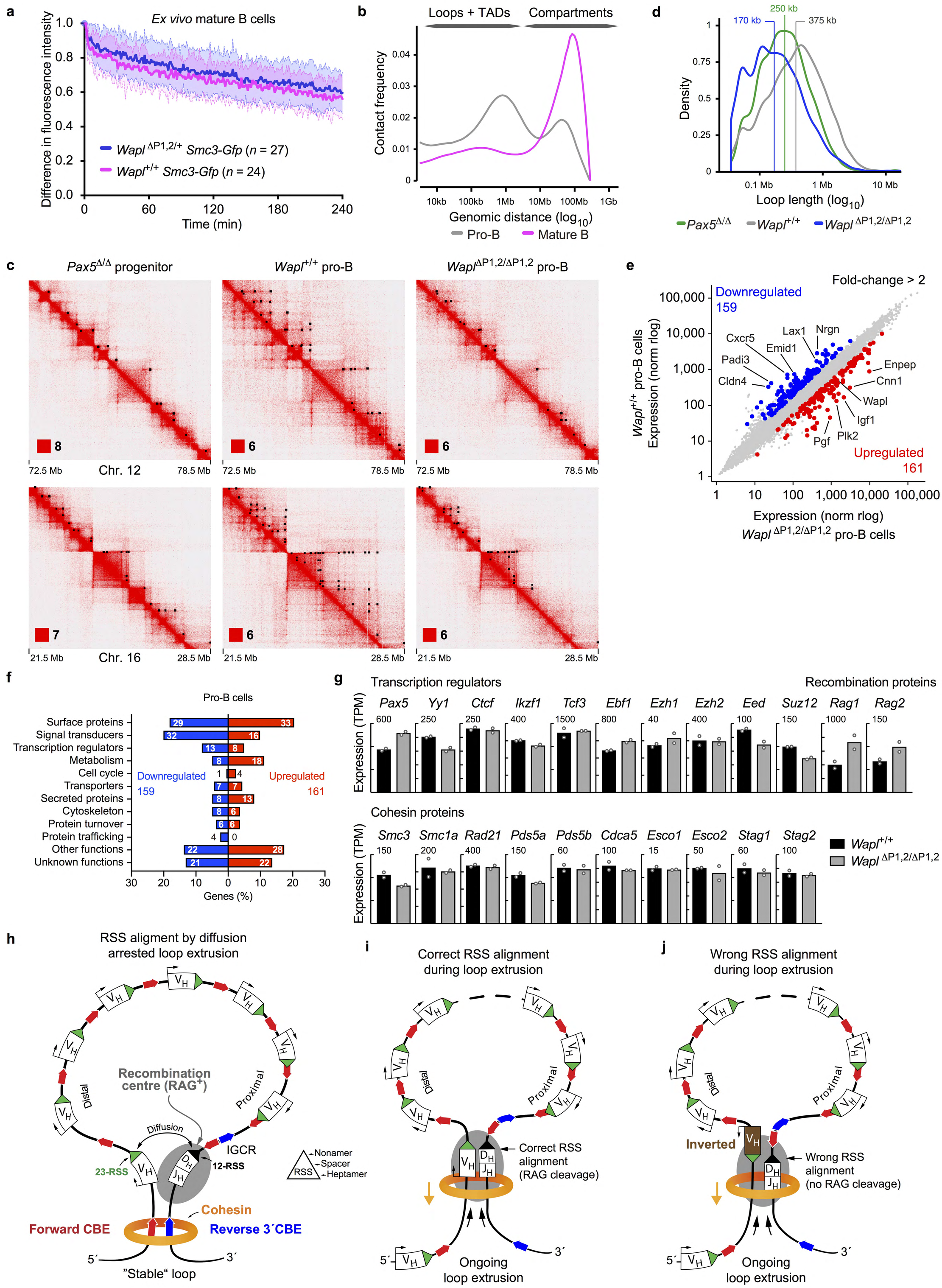
a
Ex vivo mature B cells
Difference in fluorescence intensity
Time (min)
Wapl ΔP1,2/+ Smc3-Gfp (n = 27)
Wapl+/+ Smc3-Gfp (n = 24)
b
Loops + TADs
Compartments
Contact frequency
Genomic distance (log10)
Pro-B
Mature B
d
250 kb
170 kb
375 kb
Density
Loop length (log10)
Pax5Δ/Δ
Wapl+/+
Wapl ΔP1,2/ΔP1,2
c
Pax5Δ/Δ progenitor
Wapl+/+ pro-B
WaplΔP1,2/ΔP1,2 pro-B
Chr. 12
Chr. 16
e
Fold-change > 2
Downregulated
159
Upregulated
161
Wapl+/+ pro-B cells Expression (norm rlog)
Expression (norm rlog)
Wapl ΔP1,2/ΔP1,2 pro-B cells
Cxcr5
Lax1
Nrgn
Emid1
Padi3
Cldn4
Enpep
Cnn1
Wapl
Igf1
Plk2
Pgf
f
Pro-B cells
Surface proteins
Signal transducers
Transcription regulators
Metabolism
Cell cycle
Transporters
Secreted proteins
Cytoskeleton
Protein turnover
Protein trafficking
Other functions
Unknown functions
Downregulated
159
Upregulated
161
Genes (%)
g
Transcription regulators
Recombination proteins
Pax5 Yy1 Ctcf Ikzf1 Tcf3 Ebf1 Ezh1 Ezh2 Eed Suz12 Rag1 Rag2
Cohesin proteins
Smc3 Smc1a Rad21 Pds5a Pds5b Cdca5 Esco1 Esco2 Stag1 Stag2
Expression (TPM)
Wapl+/+
Wapl ΔP1,2/ΔP1,2
h
RSS aligment by diffusion arrested loop extrusion
Recombination centre (RAG+)
Distal
Proximal
Diffusion
IGCR
23-RSS
12-RSS
Nonamer
Spacer
Heptamer
Cohesin
Forward CBE
Reverse 3´CBE
5´
3´
"Stable" loop
i
Correct RSS alignment during loop extrusion
Correct RSS alignment (RAG cleavage)
Ongoing loop extrusion
j
Wrong RSS alignment during loop extrusion
Inverted
Wrong RSS alignment (no RAG cleavage)
Ongoing loop extrusion